Journal Pre-proof

The Recent Progress of MXene-Based Microwave Absorption Materials

Zhiwei Zhang, Zhihao Cai, Yi Zhang, Yaling Peng, Ziyuan Wang, Lun Xia, Suping Ma, Zhanzhao Yin, Ruofeng Wang, Yishu Cao, Zhuo Li, Yi Huang

PII: S0008-6223(20)31237-9

DOI: https://doi.org/10.1016/j.carbon.2020.12.060

Reference: CARBON 15971

To appear in: *Carbon*

Received Date: 23 November 2020

Accepted Date: 19 December 2020

Please cite this article as: Z. Zhang, Z. Cai, Y. Zhang, Y. Peng, Z. Wang, L. Xia, S. Ma, Z. Yin, R. Wang, Y. Cao, Z. Li, Y. Huang, The Recent Progress of MXene-Based Microwave Absorption Materials, *Carbon*, https://doi.org/10.1016/j.carbon.2020.12.060.

Graphical abstract

It is necessary to develop the microwave absorbing materials (MAM) because of the electromagnetic wave (EMW) pollution has a great impact on human beings.

In this review, we summarized the features of MXene, the theories of microwave absorption (MA) and the latest progress of MXene and MXene-based composites as MAMs. Through the summary of MXene and MXene-based composites, the advantages and shortcomings of the MXene-based as high performance MAMs are presented. Moreover, the future research direction of MXene and MXene-based MAMs also has been discussed in detail.

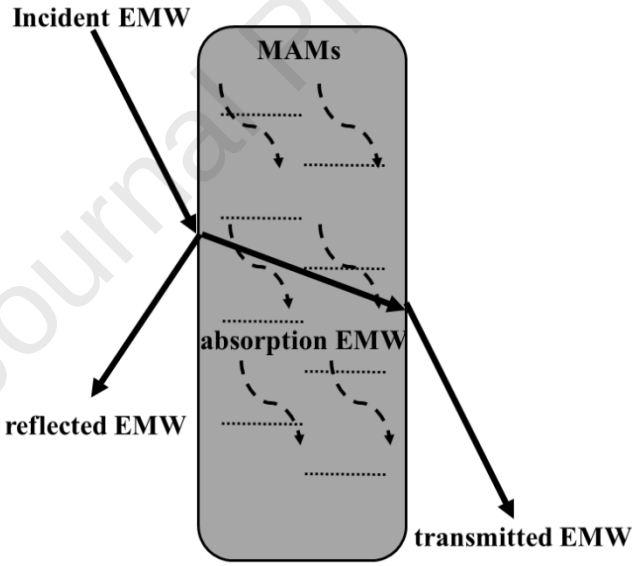

The Recent Progress of MXene-Based Microwave Absorption Materials

Zhiwei Zhang[1], Zhihao Cai[1], Yi Zhang[2], Yaling Peng[1], Ziyuan Wang[1], Lun Xia[1], Suping Ma[1], Zhanzhao Yin[1] , Ruofeng Wang[1] , Yishu Cao[1] , Zhuo Li[1] and Yi Huang[1]*

1 National Institute for Advanced Materials, Tianjin Key Laboratory of Metal and Molecule Based Material Chemistry, Key Laboratory of Functional Polymer Materials, Collaborative Innovation Center of Chemical Science and Engineering (Tianjin), School of Materials Science and Engineering, Nankai University, Tianjin 300350, China.

2 Beijing Institute of Aeronautical Materials, Beijing 100095, China

* Corresponding author. Tel: 022-2350-2604 E-mail: yihuang@nankai.edu.cn

Abstract

The development of advanced microwave absorption materials (MAMs) is a considerably important topic because our living environment is full of with electromagnetic wave pollution which threatens people's health. And MAMs are also used in radar stealth technologies for prevent the weapons from being detected. Based on the importance of MAMs in both military and civil fields, many nanomaterials have been studied as MAMs but not all of them have the satisfactory performance. MXene, a new family of two-dimensional (2D) material, has the favorable structures and properties such as special layered structure, abundant functional groups, high electrical conductivity and high specific surface area, which make it an appropriate candidate as high-performance MAMs. In this review, we summarized the features of MXene, the theories of microwave absorption (MA) and the latest progress of MXene and MXene-based composites as MAMs. Through the summary of MXene and MXene-based composites, the advantages and shortcomings of the MXene-based as high performance MAMs are presented. Moreover, the future research direction of MXene and MXene-based MAMs also has been discussed in detail.

Keywords:

MXene-based; Microwave absorption material; Reflection loss;

Effective absorption bandwidth

Content

1、Introduction

The rapid development of information technology makes great convenience to human' s life. According to media reports, 2020 is the first year of 5G (5th generation mobile networks) telecommunication outbreak. 5G has brought us disruptive experience such as ultra-high Internet speeds, driverless cars, VR (virtual reality) technology [1-4]. However, when we enjoy the convenience brought by technology, the unwanted electromagnetic wave (EMW) pollution which comes from the wireless communication equipment is threatening the human's health[5-7]. In the modern wars, many advanced aviation are the hit targets for the enemy. So stealth technology is the crucial solution to evade detection of the radar. Coating microwave absorption materials (MAMs) on military equipment is an effective anti-detection method[8-10]. Not only the human's health and the military equipment are interference by EMW, the precise instrument, information safety and device chip are also influenced by EMW pollution[11-13]. For these situations, the design and development of high-performance MAMs is considered to be the most effective method to solve these problems.

The traditional MAMs mainly include carbon-based materials[14-15], ceramics[16-17], polymers[18-19], carbonyl iron[20-21], magnetic metal powder[22-23], two-dimensional (2D)nanomaterials[24-28] and so on. Dielectric loss materials are represented by carbon-based materials, ceramics, polymers and so on. The features are high strength, resistance to high temperature, excellent electrical conductivity and low density, but effective absorption bandwidth (EAB) and the MA performance is not sufficient. Magnetic loss materials are represented by carbonyl iron, ferrite and magnetic metal powder. However, their high density and poor stability limit their practical application. The traditional MAMs are not

sufficient with the rapid development of science and technology, and “thin, wide, light and strong” is the developing direction of high-performance MAMs[29-31]. Therefore, many scholars devote themselves to developing novel materials for MAMs.

In the process of studying high-performance MAMs, 2D nanomaterials have the special structures and properties such as large aspect ratios, large specific surface area, good conductivity, abundant functional groups, low density, good thermal stability, flexibility and mechanical strength [32-33], attracting extensive attention worldwide. These advantages make them strong dielectric loss, polarization loss and multiple reflections inside the nanomaterials compared to other MAMs. Thus, the 2D materials have wide application prospects in the field of MAMs.

MXene, a new family of 2D materials, which was discovered by Yury Gogotsi in 2011[34]. MXenes are synthesized from selecting etching “A” layers from MAX phases($M_{n+1}AX_n$, M represents transition metals, A represents elements from III–VI group, X represents C and/or N) [34-35]. So far, more than 20 types of MXenes with different transition metals have already been synthesized, and approximately 70 different MXenes have been proposed theoretically, not counting millions of solid solutions possible in various M−X systems[36].

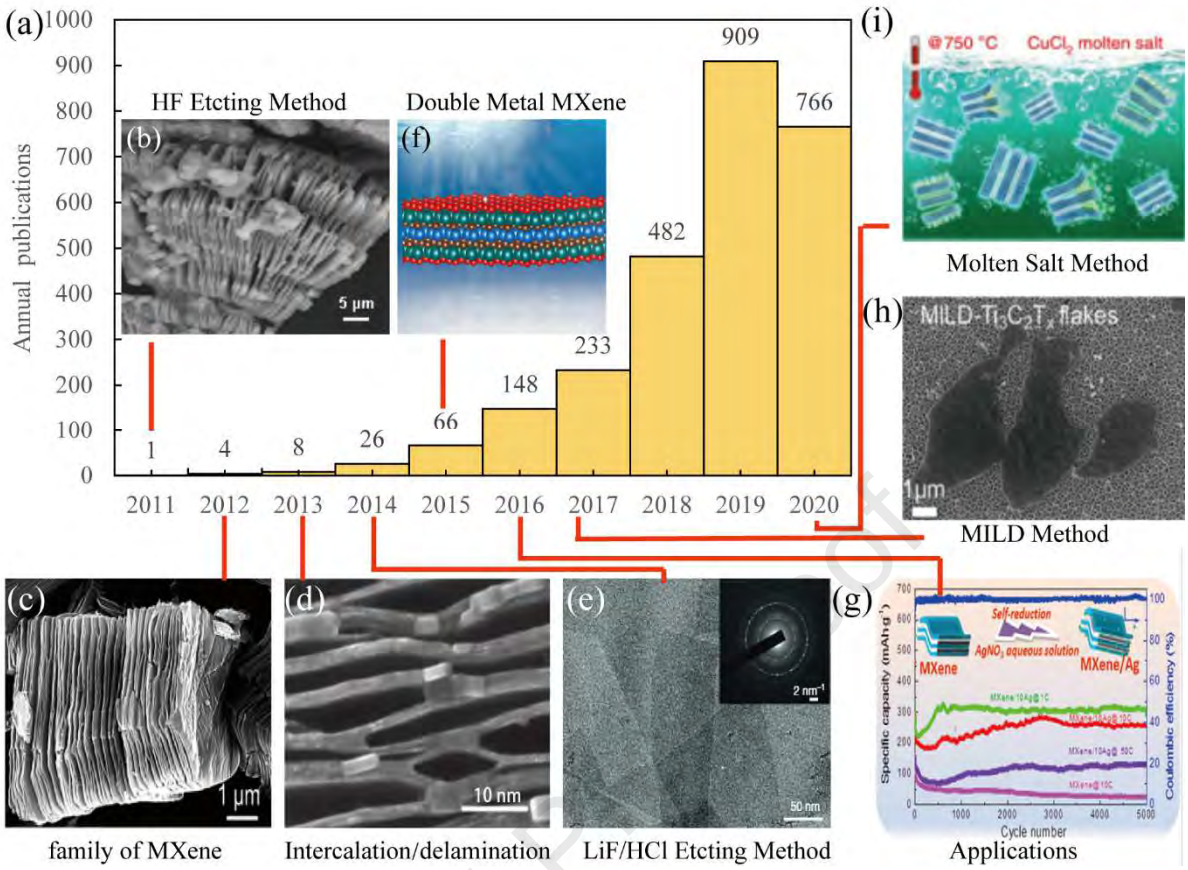

Figure 1. Trends of MXene research (2011–now). (a) Journal publications and worldwide patents issued per year, data queried from Web of Science. (b) In 2011, the multilayered $Ti_3C_2T_x$ MXene was first synthesized by selective etching of Al from Ti_3AlC_2 using HF acid[34]. Reprinted with permission. Copyright 2011 WILEY□VCH. (c) In 2012, various of MXenes have been synthesized[35]. Reprinted with permission. Copyright 2012, American Chemical Society. (d) In 2013, organic molecules have been intercalated and delaminated in layers of MXenes [37]. Reprinted with permission. Copyright 2013, Springer Nature. (e) In 2014, single flakes of $Ti_3C_2T_x$ was synthesized by HCl/LiF method[38]. Reprinted with permission. Copyright 2014, Springer Nature. (f) In 2015, double metal MXene was discovered[39]. Reprinted with permission. Copyright © 2020 American Chemical Society.(g) Many applications have been emerged such as energy storage[40], microwave absorbing material, sensor and so on. Reprinted with permission. Copyright 2016 American Chemical Society.(h) In 2017, $Ti_3C_2T_x$ MXene was synthesized by MILD method[41]. Copyright 2017 American Chemical Society. (i) In 2020, a general Lewis acidic etching route was discovered for preparing MXenes[42]. Reprinted with permission. Copyright 2020, Springer Nature.

MXene has been studied for nearly ten years, the research process is shown in Figure 1. The structural features of MXene is abundant functional groups (OH, O and/or F groups), single-layer or multi-layer structure. And MXene has also shown many outstanding physical and chemical properties such as hydrophilic surface, and high conductivity. And if “M” is Cr

and/or Mn, e.g., Cr_2AlC, Cr_2GeC, Cr_2GaC, Cr_2AlN, Mn_2AlC, Mn_2GaC, Cr_2TiAlC_2, and $(Cr_{2/3}Sc_{1/3})_2AlC$, this type of MXene can exhibit magnetic properties[43]. These characteristics mentioned above enable MXene to be applied in energy storage[44-45], desalination[46-47], sensor[48-49], catalysis[50-51], film[52-53], electromagnetic wave interference shielding[54-55] or absorption[56-57] and so on. In this review, we will only focus on the application of MXene to EMW absorption.

Due to the many advantages of MXene, it attracts much attention in the field of MA. The structural, physical and chemical properties diversity of MXene makes the optimization of its MA performance more selective. Firstly, many defects can be brought in the synthesis process of MXene, these defects can introduce interfacial polarization and enhance the MA performance. Secondly, the abundant functional groups of the MXene make it easier to compound with other loss materials, thus the improvement and control of the MAMs can be realized. Thirdly, the larger layer spacing can make the EMW multiple reflections and scattering. Furthermore, the high conductivity endows MXene-based MAMs strong dielectric loss and polarization loss. Similar to graphene, the 2D MXene can be an ideal substrate material to couple with other loss materials in order to further improve the MA performance.

In order to further improve the MA performance of MXene, other dielectric and magnetic materials are often incorporated with MXene. In this review, we will discuss the recent progress of MXene and MXene-based MAMs, including pure MXene, MXene/dielectric materials, MXene/magnetic materials and MXene/multiple loss materials. Through performance analysis of different kinds of MXene-based MAMs, the design method of high-performance MAMs can be used for reference. And the shortcomings of present and

some perspectives on future MAMs development are provided.

2、Preparation and properties of MXene

Up till now, more than 70 kinds of MAX have been discovered and nearly 20 MXenes have been synthesized successfully. As we know, the M-A bond in the MAX phase is weaker than M-X bond, so the atom reactivity of layer A is relatively high and they can be broken easily. Though the M-A bond is weaker than M-X bond, it is still stronger than van der Walls interaction and more difficult to break M-A bond than graphene by mechanical exfoliation[58-59]. At present, the most commonly used method is the chemical method to etch MAX in order to obtain MXene.

2.1 Preparation of MXene

2.1.1 HF acid etching

In 2011, MXenes ($Ti_3C_2T_x$) were prepared from Ti_3AlC_2 by selective etching Al with HF acid for the first time[60]. The etching reaction equations are as follows:

$$Ti_3AlC_2 + 3HF = Ti_3C_2 + AlF_3 + 3/2H_2 \quad (1)$$

$$Ti_3C_2 + 2H_2O = Ti_3C_2(OH)_2 + H_2 \quad (2)$$

$$Ti_3C_2 + 2HF = Ti_3C_2F_2 + H_2 \quad (3)$$

This is the most common way to synthesize MXene. The quality of MXene is determined by the HF concentration, reaction time, reaction temperature, the size of MAX and so on. The resultant Ti_3C_2 MXene are terminated with abundant –F, –O, and/or –OH functional groups because the etchant solution is rich in fluorine anions and hydroxyl groups[61-63]. After etching, the metallic Ti-Al bonds are replaced by weak bonds such as hydrogen and van der Waals bonds. The weak bond between the synthesized multi-layer MXene could be

delaminated into single layer or a few layers by a sonication process or even manual shaking. The intercalation agents such as DMSO, tetrapropylammonium hydroxide (TPAOH), tetramethylammonium hydroxide (TMAOH) urea and other materials are usually used to insert into the interlayer of multi-layer MXene so as to obtain single layer or a few layers MXene[64-66]. In addition, the HF acid used in the experiment is highly toxic and corrosive, which is certain risks in actual operation.

2.1.2 Fluoride Salt Etching

HF acid etching method is relatively dangerous and requires intercalation agents for further insertion steps, while MXene etched by LiF/HCl is a mild process and Li^+ can be viewed as intercalation agents which can enlarge MXene layer spacing and weakens the interlayer interaction. The multi-layer MXene more easily delaminated during sonication and obtaining single or few-layer of MXene flakes. The etching reaction equations are as follows[67]:

$$2Ti_3AlC_2 + 6LiF + 6HCl = 2Ti_3C_2 + Li_3AlF_6 + AlF_3 + 3LiCl + 3H_2 \quad (4)$$

The Fluoride salt etching method is similar to the HF acid method, but easier, safer and higher efficiency than the HF acid method. Similarly, NaF, KF, CsF, $[(C_4H_9)_4NF]$, CaF_2 mixed with HCl or H_2SO_4 can also replace the HF[68]. The ratio of LiF to HCl is an important parameter to produce high-quality MXenes nanosheets in high yield. The surface functional groups of $Ti_3C_2T_x$ (T=OH, O, F) have great influence on the properties.

2.1.3 Molten salt etching

With the molten salt method to etch MAX, the layered MXene can be avoided being broken in hazardous environment, and also safer to the experimenter. Yury's group used a molten fluoride salt (KF, NaF and LiF) to etch Al from Ti_4AlN_3 precursor at 550°C in Ar to synthesis

the MXene Ti_4N_3[69]. In order to get delaminated MXene, TBAOH was acted as intercalation agent. Recently, Lin and et.al proposed a redox-controlled A-site etching of MAX phases in Lewis acidic melts and some unconventional MXene had been synthesized with A elements Si, Zn and Ga[70]. $Ti_3C_2T_x$ MXene synthesis from the reaction between Ti_3SiC_2 and $CuCl_2$ at 750 °C; this synthesis involves the following reactions:

$$Ti_3SiC_2+2CuCl_2=Ti_3C_2+SiCl_4+2Cu \quad (5)$$

$$Ti_3C_2+CuCl_2=Ti_3C_2Cl_2+Cu \quad (6)$$

The formation mechanism of $Ti_3C_2Cl_2$ from Ti_3SiC_2 is similar to the chemical etching of Ti_3AlC_2 in HF solution. Cu^{2+} and Cl^- act as H^+ and F^-, respectively.

Through the introduction of the different etching methods above, each method has its own applicable conditions and characteristics. The HF acid and Fluoride salt etching are the main methods for preparing MXene. Researchers use HCl-LiF more often to prepare delaminated MXene because the HF acid etching method is relatively risk and additional step is required to obtain delaminated MXene. Molten salt etching is the safest etching method at present. It can etch the unconventional MAX material, but the temperature is higher and the etching yield is lower.

2.2 Properties of MXene

2.2.1 Electrical conductivity

The most important feature of MXene is the considerable electrical conductivity. Some studies show that the conductivity of $Ti_3C_2T_x$ MXene could achieve high value. Table 1 gives a summary of the electrical conductivity with different MXenes recently reported. MXene always keeps high conductivity regardless of its synthesis and treatment methods. The

electrical conductivity of MXenes is usually determined by many factors such as functional groups, the size of MXene, defect, and contact resistance between nanosheets.

Table 1 The summary conductivity of MXene

Name	Description	Conductivity (S cm^{-1})	Ref.
monolayer $Ti_3C_2T_x$flakes	a modified synthetic method	4600 ± 1100	[71]
highly transparent and conductive $Ti_3C_2T_x$ films	spin-casting of Ti_3C_2Tx nanosheet colloidal solutions, vacuum annealing at 200 °C	9880	[72]
pure $Ti_3C_2T_x$ films	single-layer nanosheets	2400	[73]
post-treatments Ti_3C_2 nanosheets	Post-treatments of alkalization and calcination	2140	[74]
Solution-Processed Ti_3C_2 Films	assembled from aqueous solutions into optical quality	6500	[75]
$Ti_3C_2T_x$ films	processed into films	4600	[54]
$Ti_3C_2T_x$ films	electrophoretic deposition	7400	[52]
Delaminated $Ti_3C_2T_x$ flakes	using etchant of HCl + LiF	2000	[76]

2.2.2 Dielectric properties

The variations of dielectric properties of MXenes usually coupled with the changes of the electrical conductivity. The effect of etching time[77-78], etching temperature[79] and other treatment [80]which would improve the electric conductivity and dielectric constant is increasing at the same time.

Be incorporated with other dielectric materials is an effective way to improve the dielectric performance of MXene. This will be explained in details below. The increasing of the dielectric properties of MXenes can effectively improve the MA performance, but too high permittivity will cause impedance mismatch, which will reduce MA performance.

2.2.3 Magnetic properties

The main attenuation mechanism of MXene is dielectric loss. And the magnetic loss is very

weak. The permeability of MXenes didn't change with the frequency in the electromagnetic field. As mentioned above, if "M" is Cr and/or Mn, this type of MXene can exhibit magnetic properties. But most of the MXenes are dielectric loss materials. The introduction of magnetic materials is an effective mean to improve impedance match, which will benefit to the MA performance.

2.2.4 Others

MXene, a new kind of 2D material, has high electrical conductivity, abundant functional groups, surface defects, large specific aera, and act as dielectric loss material[81-82]. However, MXene has poor antioxidant performance in air or in oxygen-containing solution. The oxidative product of MXene is TiO_2, which is also a typical dielectric loss material. As usual, the MXenes should be kept in dark with anaerobic environment. But sometimes, part of MXene converted into TiO_2, the impedance matching will be improved, which is beneficial to the MA performance.

3、The theories of Microwave Absorption and Attenuation

EMW is a kind of oscillating particle wave derived from the electric field and magnetic field in the same direction and perpendicular to each other in space. This action is in accordance with Maxwell's equations[83-84]. When the EMW enters into lossy material, the incident EMW can be divided into three parts: the reflected EMW, the absorbed EMW and the transmitted EMW.

Dielectric loss and magnetic loss are the main routes for MAMs to attenuate EMW. Impedance matching and electromagnetic attenuation capability are two important criteria for the EMW absorption. Relative complex permittivity and relative complex permeability are

two main parameters in the field of MAMs, where ε′ or μ′ are associated with energy storage, and ε" or μ″ stands for the energy dissipation. [85-87]

$$\varepsilon_r=\varepsilon' - j\varepsilon'' \quad (7)$$

$$\mu_r= \mu' - j\mu'' \quad (8)$$

The dielectric and magnetic loss factors, defined as $tan\,\delta_E = \varepsilon''/\varepsilon'$and $tan\,\delta_M = \mu''/\mu'$, are suggested to evaluate dielectric and magnetic losses[88-90].

Based on the ε_r and μ_r, the reflection loss (RL) values were calculated according to transmission line theory, the equations were as followed[91-93]:

$$R_L = 20log|(Z_{in} - Z_0)/(Z_{in} + Z_0)| \quad (9)$$

$$Z_{in} = Z_0\sqrt{u_r/\varepsilon_r}\,tanh[j(2\pi fd/c\sqrt{\varepsilon_r u_r})] \quad (10)$$

In the formula, Z_0 is the impedance of free space (377 Ω), Z_{in} is the input impedance, f is frequency, d is the thickness of the samples, c is the velocity of light. For practical application, the RL is usually ≤−10 dB, which means that over 90% of incident EM wave could be absorbed. As Z_{in}/Z_0≈1, that is , the input impedance and the free space impedance are perfectly matched, and the incident EMW can completely enter the inside of the MAMs. It can be effectively consumed or converted into thermal or other kinds of energy.

3.1 Dielectric loss

Dielectric loss has the characteristic that electronic interacts between the electric field of the incident EMW and the nanomaterial which results in reflection loss. The dielectric loss ability is mainly derived from electric conductivity loss and polarization relaxation loss [94-95].

The electric conductivity loss is that when the EMWs enter into the MAMs, the charge carriers would form a current under the action of the electric field, then dissipated out.

The polarization relaxation loss is split into ionic polarization, electronic polarization, dipoles relaxation polarization and interfacial polarization (spatial polarization)[96]. Ion polarization is caused by the relative displacement of anions and anions. Electron polarization is caused by position change of the constituent atoms relative to the nucleus, thus the dipole moment is generated. Ion polarization and electron polarization usually occur in the frequency range of ultraviolet, visible and infrared light, which is much higher than the microwave frequency range (2~18GHz), so they are usually excluded. Dipoles relaxation polarization, refers to the polarization which is caused by the rotation of the dipole moment in the direction of the electric field. The relaxation loss can be analyzed by Debye equation[97-99]:

$$\varepsilon' = \varepsilon_\infty + (\varepsilon_S - \varepsilon_\infty)\frac{1}{1+\omega^2\tau^2} \tag{11}$$

$$\varepsilon'' = (\varepsilon_S - \varepsilon_\infty)\frac{\omega\tau}{1+\omega^2\tau^2} \tag{12}$$

We can deduce an equation from (3) and (4) as follows:

$$\left(\varepsilon' - \frac{\varepsilon_S+\varepsilon_\infty}{2}\right)^2 + (\varepsilon'')^2 = \left(\frac{\varepsilon_S-\varepsilon_\infty}{2}\right)^2 \tag{13}$$

Where ε_S is the static dielectric constant and ε_∞ is the dielectric constant of infinite frequency, τ is the time of relaxation. The circle of this equation is called Cole-Cole semicircle. The points on the semicircle correspond to the values of the real and imaginary parts of the dielectric constant at a certain frequency calculated by the Debye equation. Each Cole-Cole semicircle represents a polarization relaxation process[100-102]. Interfacial polarization usually appears at the interface of heterogeneous medium, which is caused by the accumulation of electrons or ions at the interface under the action of the external electric field[103-104].

3.2 Magnetic loss

Magnetic loss refers to the phenomenon that the work done by the outside world to a magnetic material is converted into heat during the process of magnetization or demagnetization. It includes hysteresis loss, eddy current loss and residual loss[105-106].

The hysteresis loss is due to the hysteresis loop relationship between the magnetic perceptual strength and the magnetic field strength[107-108].

The eddy current loss is caused by the induced current in the conductor when a conductor moves in an inhomogeneous magnetic field or is in a time varying magnetic field. It can be defined as[109-111]:

$$C_0 = \frac{\mu''}{(\mu')^2 f} = \frac{2}{3}\pi\mu^0\delta d^2 \quad (14)$$

where δ is the electrical conductivity of material, d is the thickness of the MAMs. From the equation, C_0 is a constant at a certain thickness of the MAMs with the change of frequency. This is one of the ways to determine whether EMW loss only results from the eddy current loss.

The residual loss refers to other losses except hysteresis loss and eddy current loss. The multiple loss material is not just a single loss mechanism, it combined the advantages of various losses.

3.3 Other theories

We all know that the synergistic effects between the dielectric loss and magnetic loss contribute to the excellent EM wave absorption ability, which results in the good impedance matching and strong EM wave attenuation of the MAMs. However, the conflict between the two sides still exist. In order to absorb the EMW into the material as much as

possible, it will inevitably reduce the attenuation ability of the MAMs to the EMW. Therefore, it is necessary to coordinate impedance matching and EMW attenuation in practical application. The attenuation constant α can be defined [112-114]:

$$\alpha = \frac{\sqrt{2}\pi f}{c}\sqrt{(\mu''\varepsilon'' - \mu'\varepsilon') + \sqrt{(\mu''\varepsilon'' - \mu'\varepsilon')^2 + (\mu''\varepsilon'' - \mu'\varepsilon')^2}} \quad (15)$$

The quarter-wavelength matching model shows the relationship between a matching thickness (t_m) and corresponding matching frequency (f_m), it can be calculated using the following equation: [115-117]

$$t_m = nc/(4f_m\sqrt{|u_r||\varepsilon_r|}) \text{ (n=1,3,5…)} \quad (16)$$

4、MXene-Based Materials as MAMs

4.1 Pure MXene as MAMs

Although MXene has been widely studied as MAMs during the last five years, the MA performance of pure MXene is less than satisfactory. This is because the high relative complex permittivity and low relative complex permeability contribute to impedance mismatching. In Qing's work, they prepared Ti_3C_2 nanosheets with a typical MXene structure by the treatment of Ti_3AlC_2 powders in HF. And the maximum RL of -17 dB can be obtained at about 14.6 GHz with a thickness of 1.4 mm in the frequency range of 12.4–18 GHz[28], which is much stronger than pure RGO (−8.07 dB at 16.4 GHz for a thickness of 1.36 mm)[118] due to the dipole polarization induced by surface groups, the localized defects and large specific aera contributes to the dielectric loss. But the MA performance of pure MXene is far from exciting. In order to get higher MA performance, much efforts should be made to regulate the dielectric properties.

The appropriate fraction of paraffin loaded into the matrix is a small tip to optimize the MA

performance. Zhang and his co-workers mixed paraffin and $Ti_3C_2T_x$ with different proportions of 4:6, 5:5 and 6:4, and they found $Ti_3C_2T_x$-50% (5:5) presents good impedance matching and achieved with high MA performance. The effective absorption bandwidth(EAB) (RL ≤ −10 dB) between 12.4 GHz and 17.1 GHz at only 1.5 mm, and maximum RL of −34.4 dB at 12 GHz at a thickness of only 1.7 mm[119]. The fraction of paraffin is a key point to obtain better MA performance.

Much progress has been made in the synthesis of MXene during the past decade. The structures, physical or chemical properties are determined by the synthesis conditions, such as reactant concentration, reaction time and reaction temperature. The dielectric properties and MA performance are varied. Gu's group synthesized $Ti_3C_2T_x$ by tuning the reacting conditions[32]. With increasing reaction concentration, the kinetic process can be promoted during the exfoliation reaction. The ordered multilayer is determined by the reaction time. And the exfoliation degree improves considerably with increasing reaction temperature. The sample exfoliated at 45 °C for 24 h under 12 M HCl shows RL of −45.2 dB at 7.2 GHz with a thickness of only 1.5 mm. And the sample prepared with 9 M HCl at 35 °C for 24 h shows RL of −40.8 dB at 13.9 GHz and the broadest EAB, 3.66 GHz at 1.68 mm. Gu's group had published another article about the impact of diverse etching times on the structure, morphology, and dielectric properties [78]. The different interlamellar spaces of $Ti_3C_2T_x$ MXene nanosheets were prepared by HF acid etching for 1 h, 2 h and 3 h by Zhang's group[77]. The SEM images are shown in Figure 2. As the reaction time increases, the layered $Ti_3C_2T_x$ MXenes material gets thinner and more layered, and the spacing between the layers becomes larger. The test results show that the RL value is strongly dependent on interlayer

spacing. The maximum RL of S1(1h), S2(2h) and S3(3h) are -4.6 dB at 6.1GHz, -12.5 dB at 3.2 GHz and -36.3 dB at 4.67 GHz, respectively. The sample of S3 with larger interlayer spacing show a stronger MA performance due to layered structure can make EMW multiple reflections and cause scattering inside the material.

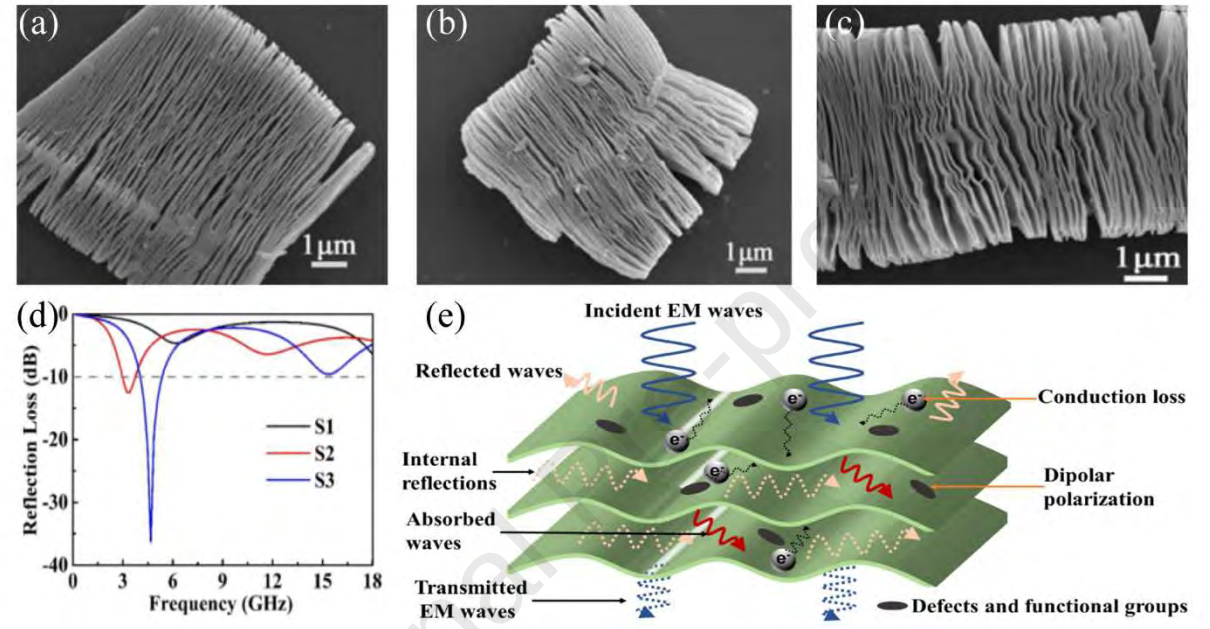

Figure 2. SEM images of $Ti_3C_2T_X$ MXene with different etching time: 1 h (a), 2 h (b) and 3 h (c). (d) RL of $Ti_3C_2T_x$ MXenes with different interlamellar space (40% paraffin, absorber thickness: 4.5 mm). (e) Absorbing mechanism diagram of two-dimensional layered $Ti_3C_2T_x$ MXenes material. Reprinted with permission. Copyright 2020, Elsevier.

MXene is easily oxidized under certain conditions, which is one of the key problems puzzling researchers. The oxidation product of MXene is TiO_2. However, in the field of MA, the oxidation process is equivalent to the introduction of TiO_2 and C in situ and the MXene/TiO_2/C can be formed. The dielectric properties and MA performance would be optimized. Generally, high temperature annealing can convert part of MXene into TiO_2. Yin prepared the derivatives of Ti_2CT_x MXene by calcined for 1 hour in a furnace at 500□, 800□ and 900 □ in a flowing CO_2 atmosphere [81]. The product of Ti_2CT_x/TiO_2, C/TiO_2, and TiO_2 at different oxidation temperatures are formed respectively. The C/TiO_2 shows the maximum

RL of -50.3 dB at 7.1 and 14.2 GHz and the EAB of 4.7 GHz at 1.45mm. Moreover, the wider EAB value of 14.5 GHz (3.1–15.5 GHz and 15.9–18 GHz) can be obtained at 5 mm ,as shown in Figure 3. The impedance matching can be optimized by the low permittivity TiO_2 flakes and they are uniformly embedded in the carbon layers, so more interfaces can be introduced. What's more, the abundant defects and functional groups induce polarization loss and EM wave dissipation. At last, the carbon layers provide more conductive paths for charge carriers to migrate results in EM wave attenuation caused by the conduction loss. The other two articles have shown the similiar experiments and conclusions[82, 120].

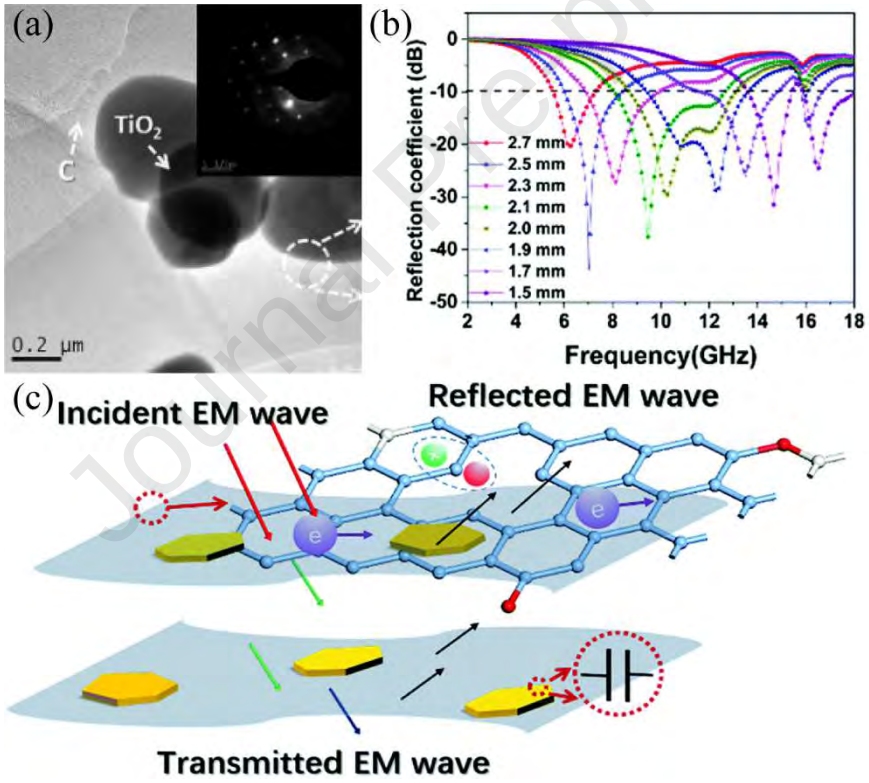

Figure 3. (a) TEM images of CO_2-800. The corresponding SAED patterns are shown in the upper insets of panels. (b) The RL versus frequency and thickness of C/TiO_2. (c) Schematic of the EM wave absorption mechanisms for C/TiO_2 composites. Reprinted with permission. Copyright 2017, The Royal Society of Chemistry.

Since pure MXene has the features of high electrical conductivity and excellent dielectric properties, the researchers usually regulate the impedance matching through a series of means such as reaction conditions or oxidation conditions. However, we have to admit that the MA

performance of pure MXene is not very satisfying. Therefore, the introduction of other dielectric loss material or magnetic loss material to improve impedance matching is the development direction of MXene-based MAMs.

4.2 MXene/dielectric loss materials as MAMs

Compared with the pure MXene as MAMs, constructing MXene-based MAMs is a common way to manipulate the MA performance and build additional loss mechanisms. The high dielectric values of MXene will lead high interface reflection and poor impedance match. So MXene often incorporate with other dielectric loss materials for improving the MA performance of MXene, such as carbon materials, conductive polymer, ceramics, which are often incorporated with MXene, and show good MA performance.

4.2.1 MXene/Carbon-based materials

Carbon-based materials include carbon black, graphite, carbon nanofibers (CNFs), carbon nanotubes (CNTs), graphene, and their derivatives. The particular properties such as high electrical conductivity, light weight, large specific surface area, environment friendly, excellent flexibility and chemical stability, they are extensively applied in the field of electromagnetic shielding and MA.

Gu's group fabricated a unique 3D porous MXene $Ti_3C_2T_x$@RGO hybrid aerogel which combines 2D MXene and RGO sheets via a hydrothermal method and freeze-drying treatment, which shows good MA performance[121]. The $Ti_3C_2T_x$@RGO aerogel exhibits a network-like hierarchical 3D structure (shown in Figure 4), which is benefit for scattering of EMW. The optimal RL reached up to -31.2 dB, and the EAB could achieve 13.1 GHz (4.9 GH-18 GHz) with a tunable thickness of 1-4 mm. The good MA performance derived from

good impedance matching adjusted by RGO. The multiple polarization also plays a major contribution to the dielectric loss. And the diverse defects and 3D interconnected porous network are benefit for interfacial polarization and multiple scattering.

Yu's group fabricated carbon nanotubes (CNTs-COOH) and Ti_3C_2 MXene hybrids which is modified by sodium alginate (CNTs/Ti_3C_2-SA) through ice-templated freeze-drying method[122]. When the content of the hybrids amounts 40 mg/cm^3, the RL of sample is -40.0 dB. When the sample thickness of 3.95 mm, the RL reaches -24.4 dB and the EAB covers the whole X band from 8.2 to 12.4 GHz. Yin's group had also prepared $Ti_3C_2T_x$/CNT nanocomposites[123]. The RL is −52.9 dB and the EAB of 4.46 GHz at the thickness of 1.55 mm.

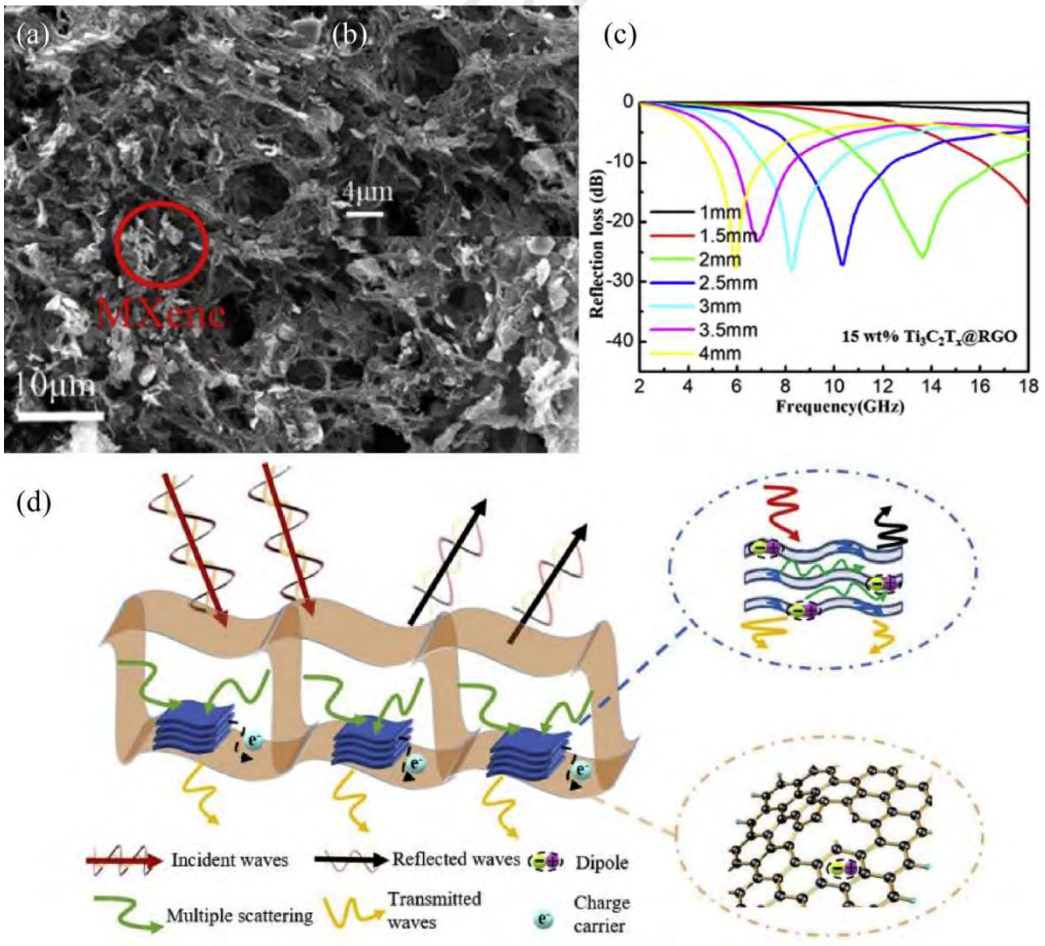

Figure 4. (a,b) SEM images of $Ti_3C_2T_x$@RGO composite. (c) RL curves of $Ti_3C_2T_x$@RGO

composite with loading 15%. (d) EM wave absorption mechanisms for $Ti_3C_2T_x$@RGO aerogel. Reprinted with permission. Copyright 2020, Elsevier.

The characteristics of multiple interfaces, electrical conductivity, defects and structural of $Ti_3C_2T_x$/carbon materials made it the excellent MA performance.

4.2.2 MXene/Polymer-based materials

The conductive polymers are often coupled with MXene for their high dielectric properties, low density, flexibility, stability and low cost. MXene/polymer composites are promising candidates in the field of MA.

Polyaniline (PANI), as a potential candidate could not only serve as protection coating, but also improve dielectric loss and impedance matching. Jiang's group prepared $Ti_3C_2T_x$ MXene/ PANI with different PANI contents[124]. The maximum RL reached −56.30 dB at 13.80 GHz with the thickness of 1.8 mm. The EAB ranges from X-band (8–12.4 GHz) to Ku-band (12.4–18 GHz) with the tunable thickness at 1.5–2.6 mm, as shown in Figure 5. The functional groups and surface defects of $Ti_3C_2T_x$ may produce dipolar polarization. PANI would also lead to conductivity loss and dielectric loss. And the synergistic effect between $Ti_3C_2T_x$ and PANI contributed to the good performance.

MXene/Polymer-based materials have the merits of interface polarization, dipole polarization, and conductive which benefit to the dielectric loss so as to improve the impedance matching.

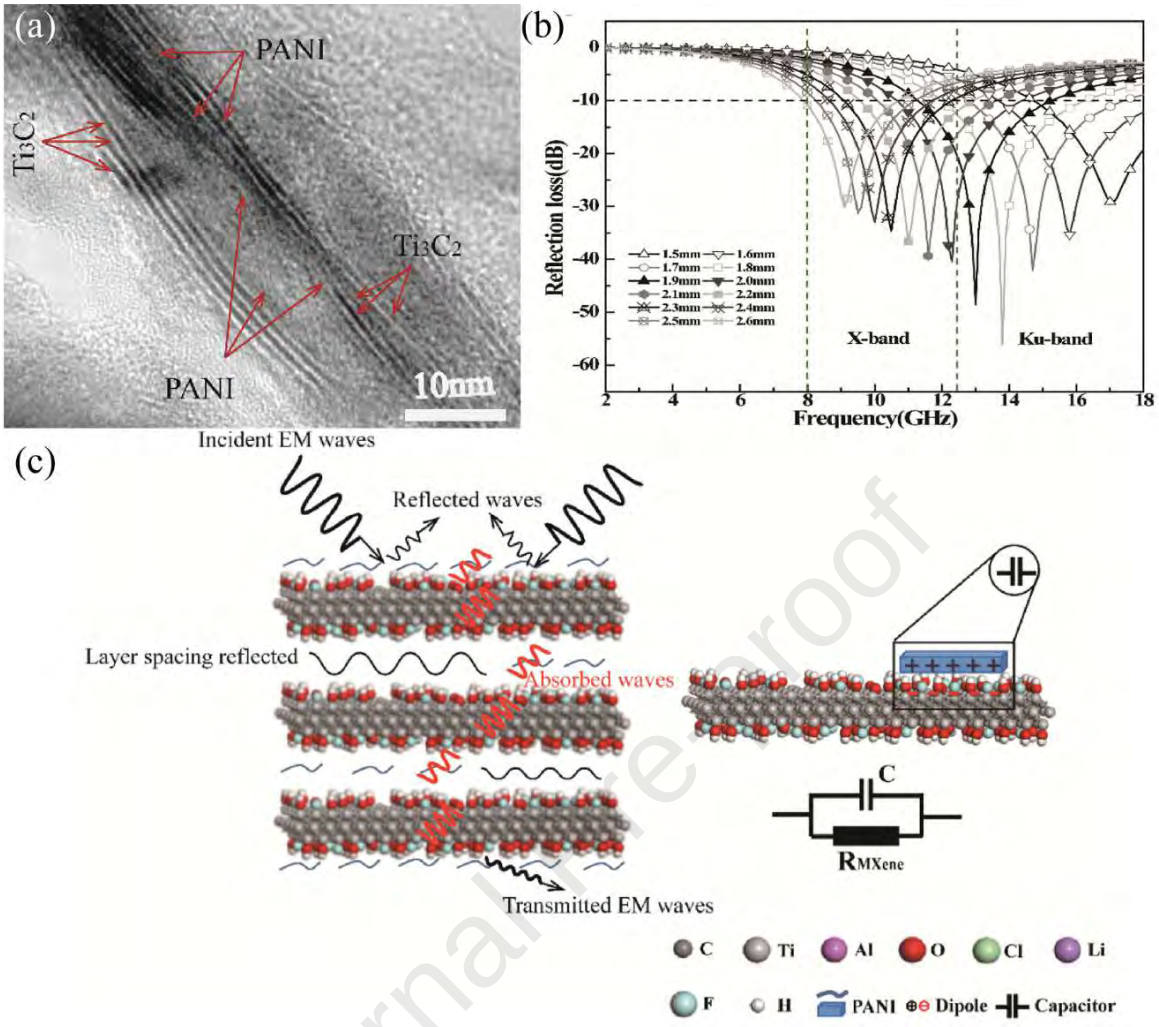

Figure 5. (a) TEM image of sample of MXene/PANI composites. (b) RL versus frequency and thickness of the sample with 50 wt% in the paraffin matrix. (c) Illustration of proposing microwave absorbing mechanism. Reprinted with permission. Copyright 2018, Elsevier.

4.2.3 MXene/Ceramic-based materials

The ceramic materials have the moderate permittivity. SiC is one of the typical ceramic material. Yin's group introduced one-dimensional (1D) defect-rich semiconductor SiC nanowires(SiCnws) with a moderate dielectric constant to balance the impedance matching and conductive loss[125]. The SiCnws were wrapped by 2D flexible MXene sheets that could not connect with each other and form a 3D network structure. And the MXene sheets can't be agglomerated because of the introduction of SiCnws. When the density of MXene/SiCnws hybrid foam is only about 0.029 $g \cdot cm^{-3}$, the maximum RL reaches up to −55.7 dB and the

EAB covers the whole X-band with the thickness of 3.5 to 3.8 mm, which is shown in Figure 6. The well match impedance characteristic and the hierarchically porous structure are benefit to the MA performance. The conduction loss and polarization loss also improve the MA properties.

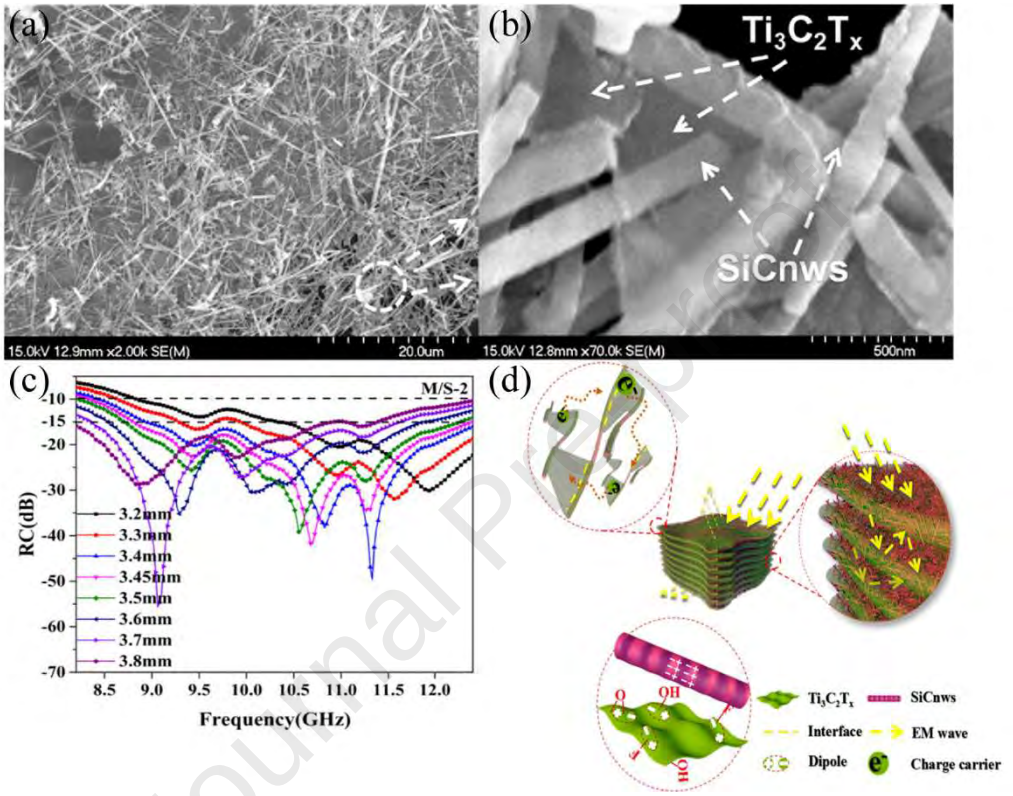

Figure 6. (a,b) Surface SEM images of $Ti_3C_2T_X$/SiCnws hybrid layers. (c) RL curves vs frequency of $Ti_3C_2T_X$/SiCnws hybrid. (d) Schematic illustrating the EM absorption mechanisms of $Ti_3C_2T_X$/SiCnws hybrid. Reprinted with permission. Copyright 2018, American Chemical Society.

4.3 MXene/magnetic loss materials as MAMs

The common magnetic loss materials include magnetic metals (Fe, Co and Ni and their alloys) and their metal oxides. When they are introduced to MXene, the high permeability of these magnetic loss materials improves impedance matching, which is benefit to MA performance.

4.3.1 MXene/magnetic metal-based materials

Li's group prepared Ti_3C_2 MXene powders with magnetic Ni particles to achieve the MA properties[102]. The Ti_3C_2/Ni has shown both the impedance matching condition and

dissipating ability. The maximum RL reached -24.3 dB at 9.8 GHz with a thickness of 2.2 mm and the EAB reached over 8.66–11.26 GHz. Feng's group had also prepared Ni@MXene hybrid and showed strong RL of −52.6 dB at 8.4 GHz, broad EAB of 3.7 GHz at thin thickness 3.0 mm with low loading 10 wt % Ni@MXene[4]. The outstanding MA performance is mainly ascribed to excellent impedance matching, the effect produced by magnetic particles, ohmic loss, multiple reflections and scattering and the formation of standing waves. Feng's group had also fabricated $Ti_3C_2T_x$ MXene/Ni Chain hybrid with excellent MA performance[103]. The RL value of −49.9 dB for the Ni-10% MXene sample was obtained at 11.9 GHz with a sample thickness of 1.75 mm. By adjusting between 1.5 and 5.0 mm, the EAB could achieve between 3.3 and 18 GHz. The excellent MA performance is mainly due to the synergistic effects induced by the permittivity of MXene sheets and the permeability of Ni chain. Similarly, MAMs such as CoFe@$Ti_3C_2T_x$[22] , $Ti_3C_2T_X$/Ni-spheres[23], FeCo-Ti_3C_2 MXene[105], Ni-modified MXene[126] and MXene/Ni nanocomposites[104] had also been reported recently.

4.3.2 MXene/magnetic metal oxide-based materials

The introduction of magnetic metal oxide into MXene is also supposed to be a feasible solution to improve the MA performance. Che's group introduced Fe_3O_4 magnetic loss material into the dielectric loss MXene, contributing to the impedance match and electromagnetic attenuation capability[127]. The maximum RL of MXene/Fe_3O_4 composites is −50.6 dB and the EAB is 4.67 GHz at only 2 mm thickness. This excellent MA performance results from the introduction of magnetic units, hollow dielectric framework, homogeneous distribution of MXene/Fe_3O_4 components, as shown in Figure 7. Similar

experiment had also been reported such as MXene/Fe_3O_4[128] and MXene/Co_3O_4[3].

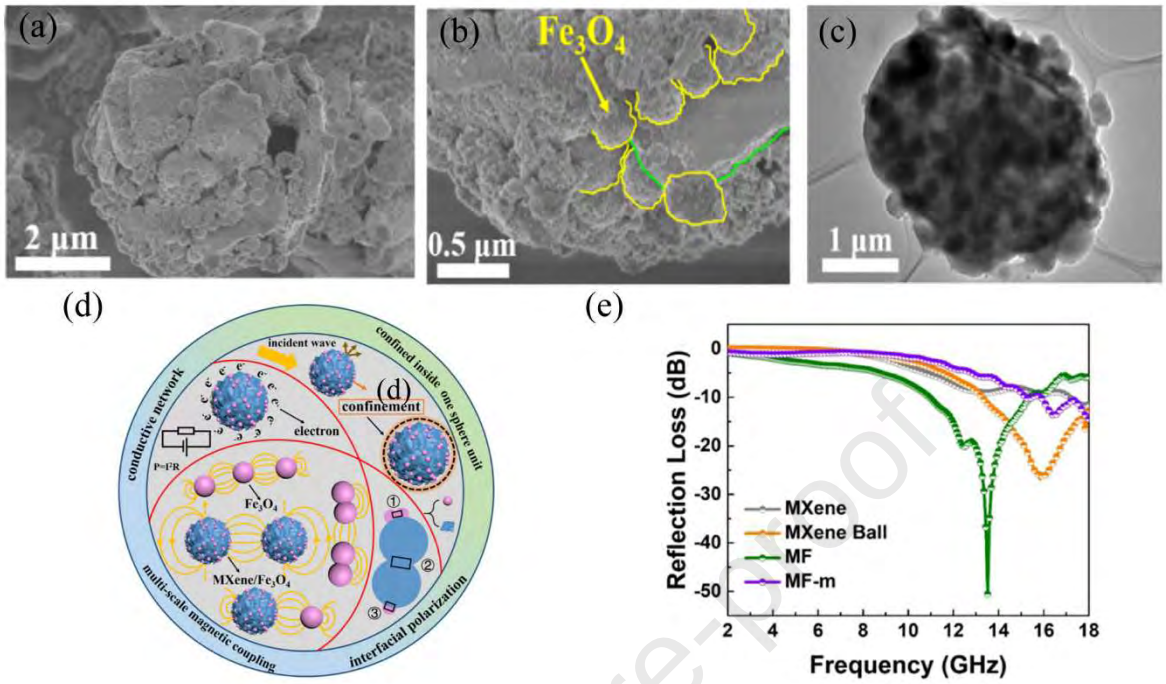

Figure 7. (a, b) SEM images of MXene/Fe_3O_4 composite. (c) TEM images of MXene/Fe_3O_4 composite. (d) Schematic illustration of MA mechanisms for the MXene/Fe_3O_4 composite. (e) RL curves about four different samples at 2 mm thickness. Reprinted with permission Copyright 2020, American Chemical Society.

As ferrites have unique magnetic property, chemical stability and low price, they have often been studied as MAMs. Kong's group prepared MXene/$Co_{0.2}Ni_{0.4}Zn_{0.4}Fe_2O_4$ (Ti_3C_2/CNZF) with various CNZF compositions through hydrothermal process [129]. The impedance matching characteristic is vital to the MA performance. The inner microwave attenuation capability also determines the MA performance. When the [$Ti_3C_2T_x$]/[CNZF] ratio was 1, the $Ti_3C_2T_x$/CNZF composite presented a maximum RL of -58.4 dB at thickness of 3.6 mm. And the EAB was about 2.2 GHz at 3.8–6.0 GHz with a thickness of 4.2 mm. Huang's group incorporated spinel nickel ferrite ($NiFe_2O_4$) with $Ti_3C_2T_x$ MXene and showed strong electromagnetic attenuation ability[130]. The MA mechanisms are summarized as follows. The defects between $Ti_3C_2T_x$ MXene and $NiFe_2O_4$ contribute to the dielectric loss. The good

electrical conductivity resulted in conductive loss. The magnetic loss from $NiFe_2O_4$. The lamellar structure generated multi-reflection effect. The $NiFe_2O_4$-$Ti_3C_2T_x$-20 sample exhibited an optimal EAB of 7.68 GHz with the material thickness of only 1.5 mm and the maximum RL is −34.0 dB at 13.92 GHz for the $NiFe_2O_4$-$Ti_3C_2T_x$-30, as shown in Figure 8. Similarly, $Ti_3C_2T_x$@$NiCo_2O_4$[131], $CoFe_2O_4$-Ti_3C_2[132] have also been reported and all of them exhibit enhanced MA performance.

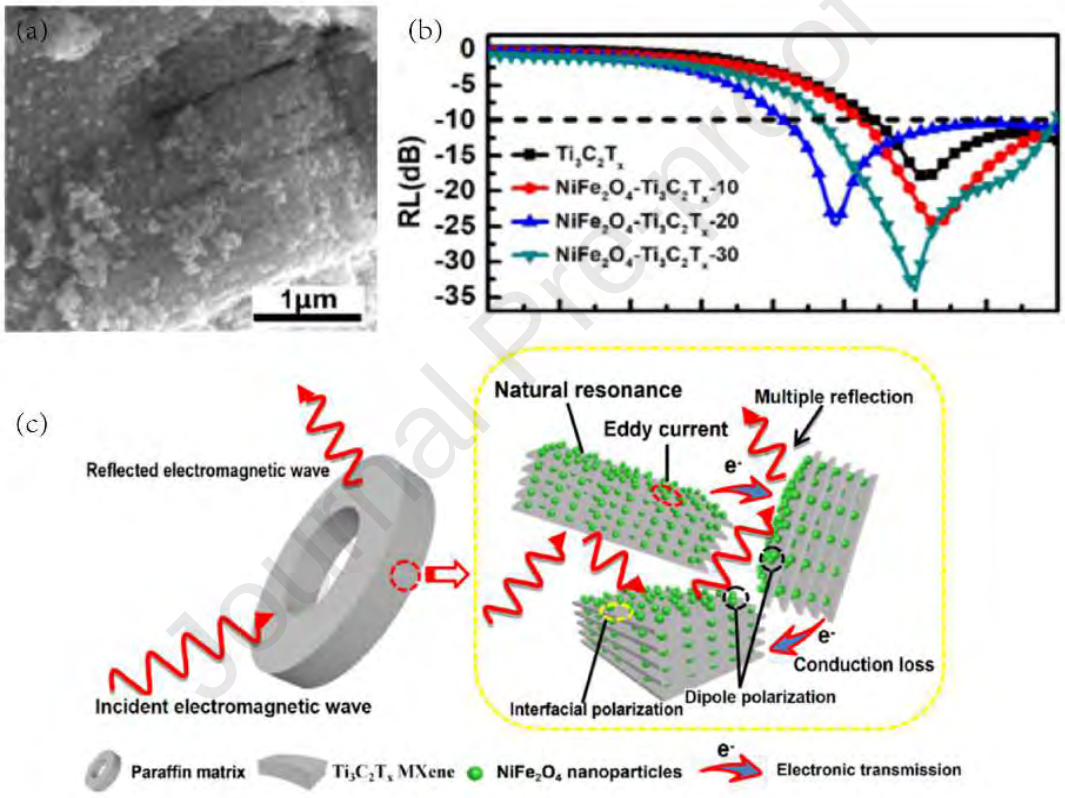

Figure 8. (a) SEM images of $NiFe_2O_4$-$Ti_3C_2T_x$-20, (b) RL values of the samples (c) Schematic illustration of microwave absorption mechanisms of the $NiFe_2O_4$-$Ti_3C_2T_x$-20 sample. Reprinted with permission. Copyright 2019, Elsevier.

4.3.3 MXene/Carbonyl iron-based materials

Carbonyl iron (CI) particles are one of the most widely used magnetic materials. As a MAM, it has many advantages such as larger values of permeability, broad absorption bandwidth, large-scale fabrication and low cost[133-135].

Qu's group fabricated the hybrid Ti_3C_2/FCI powders with different mass ratios by ultrasonic

mixing method[21]. Though the RL is not prominent, the EAB (RL < − 10 dB) of 8.16 GHz is obtained in the coating with 20 wt.% Ti_3C_2 MXene and 40 wt.% FCI loading and the thickness of 1.0 mm. The remarkable MA performance was attributed to the good impedance matching and moderate attenuation ability.

In brief, the introduction of magnetic materials such as magnetic metal, magnetic metal oxide, Ferrite and carbonyl iron, not only increases the EAB, but also improves the MA performance.

4.4 MXene/multiple loss materials as MAMs

MXene coupled with single lossy materials have exhibited the insufficient MA performance. And the low absorption intensity, relatively narrow EAB, impedance mismatch hinders their practical application. Fortunately, coupled with multiple lossy material is a better solution to adjust the chemical composition and microstructure, so as to increase the MA performance. Moreover, the multi-components in the MXene-based composites can introduce interfacial polarization and good impedance matching degree, and the morphology also has an important influence on MA performance.

Liu's group synthesized a Co-doped NiZn ferrite (CNZFO)/polyaniline (PANI) on $Ti_3C_2T_X$ MXene composite with a hierarchical structure[136]. The composite exhibited excellent MA performance with an EAB of 4.1 GHz (8.2–12.3 GHz) and a maximum RL of −37.1 dB at 10.2 GHz with a thickness of only 2.2 mm, which is shown in Figure 9. The multiple loss mechanism such as eddy current loss, natural resonance, interfacial polarization, dipole polarization, and multiple reflections of the layered structure contributed to the enhanced MA properties. The hierarchical Ti_3C_2/Fe_3O_4/PANI ternary composite was prepared by Wu's group

and the sample also show strong RL of −40.3 dB at 15.3 GHz, and the EAB is 5.2 GHz (from 12.8 to 18 GHz) at only 1.9 mm[137].

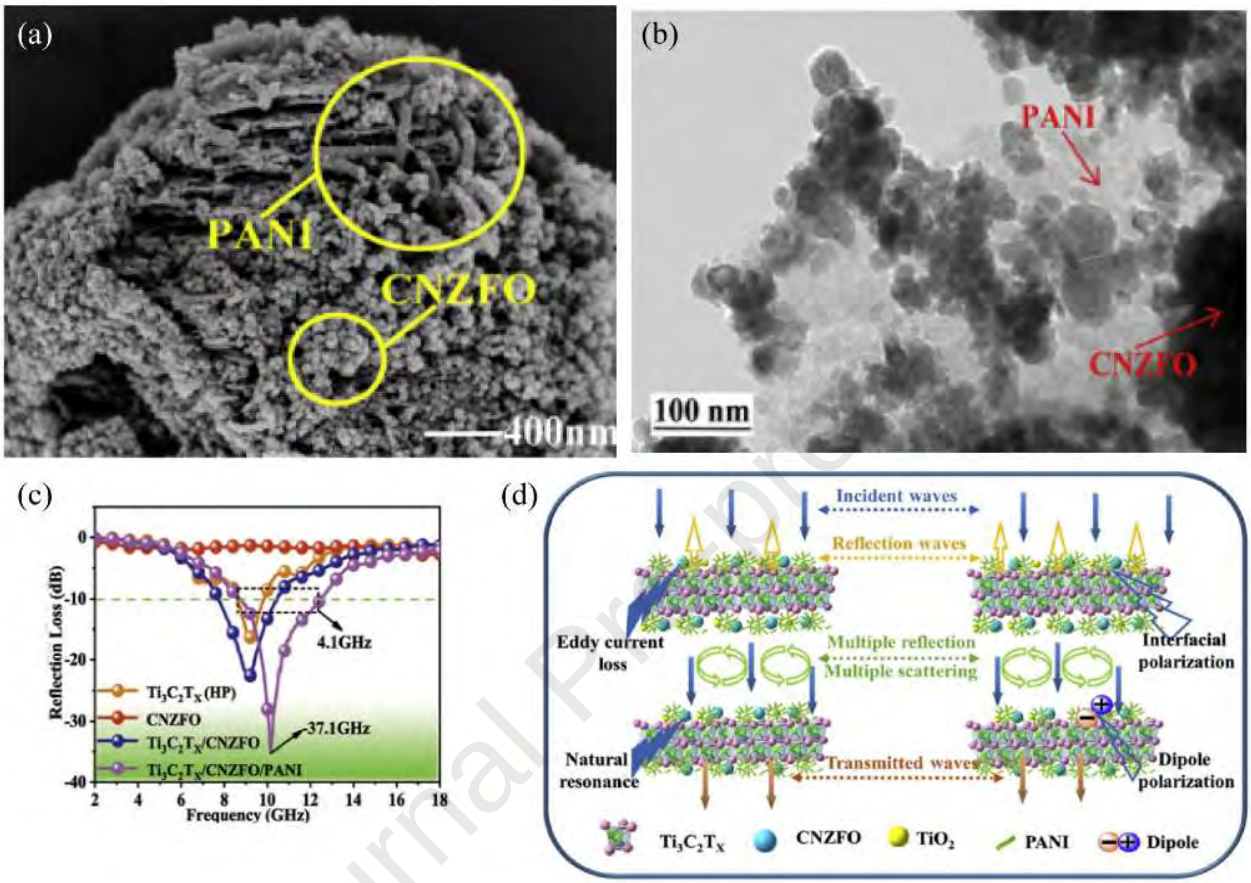

Figure 9. (a) SEM images of the $Ti_3C_2T_X$/CNZFO/PANI composite. (b) TEM images of the $Ti_3C_2T_X$/CNZFO/PANI composite. (c) RL of the samples with a thickness of 2.2 mm over the frequency range of 2–18 GHz. (d) MA mechanism for the $Ti_3C_2T_X$/CNZFO/PANI composite. Reprinted with permission. Copyright 2020, Elsevier.

Wang's group fabricated layered PVB(Polyvinyl Butyral)/Co_2Z($Ba_3Co_2Fe_{24}O_{41}$)/Ti_3C_2 MXene composite and exhibits a highly efficient MA performance [138]. Through the introduction of a ferromagnetic phase Co_2Z, the impedance match of dielectric loss and magnetic loss can be optimized. The maximum RL of PVB/Co_2Z/Ti_3C_2 composite can reach -46.3 dB at 5.8 GHz with the thickness of only 2.8 mm and the EAB is 1.6 GHz (from 4.9 to 6.6 GHz). From Figure 10b, the cole-cole semicircles of the sample PVB/Co_2Z/Ti_3C_2 composite indicated the contribution of the deby relaxation process to the enhanced dielectric properties. And the

constant values of 2-9 GHz and 13-18 GHz indicated the eddy current effect contributed to magnetic loss. The 9-13GHz attributed to the natural resonance loss, which is shown in Figure 10c.

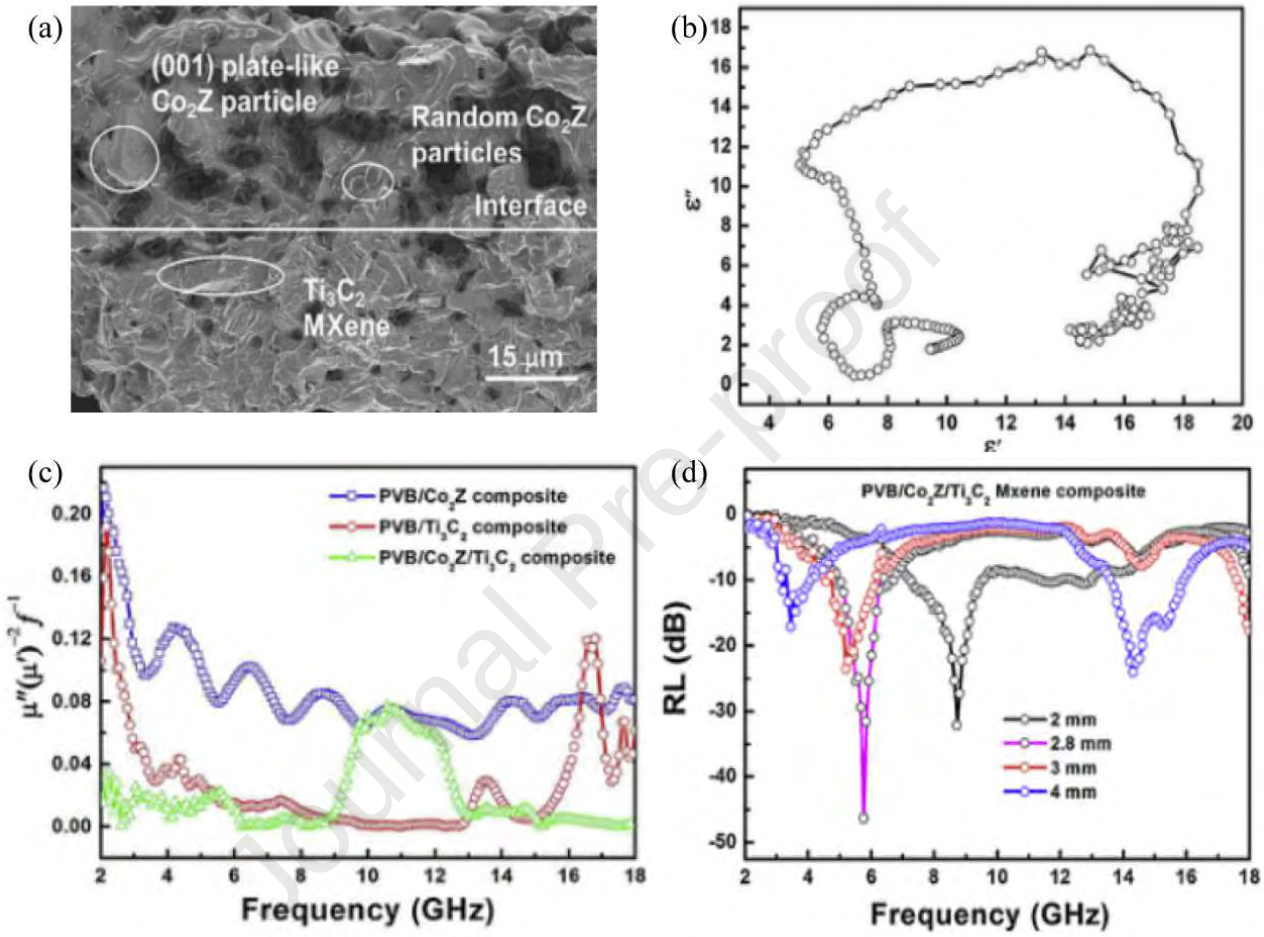

Figure 10. (a) SEM images of PVB/Co_2Z/Ti_3C_2 MXene composite. (b) Cole-Cole semicircles of PVB/Co_2Z/Ti_3C_2 MXene composite (ε' versus ε''). (c) $\mu''(\mu')^{-2}f^{-1}$ (representing eddy current loss) versus frequency of PVB/Co_2Z composite, PVB/Ti_3C_2/MXene composite and PVB/Co_2Z/Ti_3C_2Mxene composite. (d) RL of PVB/Co_2Z/Ti_3C_2 MXene composite. Reprinted with permission. Copyright 2017, Elsevier.

Besides the ternary composites composed of MXene, dielectric loss material and magnetic loss material prepared above, some other special MXene-based multiple-composites were also exploited. Liu's group synthesized Ni/TiO_2/C heterogeneous composites from $Ti_3C_2T_x$ MXene through microwave mediated reaction[139]. The maximum RL is −39.91 dB at 16.93 GHz with a thickness of only 1.4 mm. The synergistic effect of dielectric loss, magnetic loss and

unique 2D heterogeneous nanostructure contributes to the MA performance. Lu's group successfully prepared sandwich-like laminated Fe&TiO_2@C nanocomposites from the MXene–MOFs hybrids[140]. The Fe&TiO_2@C nanocomposites exhibited a broad EAB of 6.5 GHz (from 11.5 to 18 GHz) at a thickness of only 1.6 mm and the maximum RL value of −51.8 dB at 6.6 GHz at a thickness of 3 mm. The introduced rutile-TiO_2 and magnetic Fe nanoparticles improve the impedance matching which is benefit to MA performance.

When the MXene/multiple loss materials as MAMs are compared with one loss material, the introduction of both dielectric and magnetic materials can significantly improve the MA performance of MXenes, which will be the main mean of EMW attenuation.

5、Comparison of MA properties of different kinds of MXene-based MAMs

Table 2. The MA performance of different kinds of MXene-based MAMs

type	MAMs	RL_{max} (dB)	EAB(GHz)	Thickness(mm)(EAB)	Ref.
Pure MXene	Ti_3C_2 nanosheets	-17@14.6GHz@1.4mm	5.6GHz(12.4~18GHz)	1.4	[28]
	$Ti_3C_2T_x$ MXenes	-34.4@12GHz@1.7mm	4.6GHz (12.4~17GHz)	1.7	[119]
	$Ti_3C_2T_x$ MXene	-45.2@7.2GHz@1.5mm	3.66GHz	1.68	[32]
	$Ti_3C_2T_x$ MXenes	-36.3@4.67GHz@4.5mm	4 GHz (14~18 GHz)	1.5	[77]
	$Ti_3C_2T_x$ MXenes	-27.5@17.1GHz@4mm	3 GHz	2	[78]
	C/TiO_2	-50.3@7.1/14.2GHz@1.45 mm	14.5 GHz (3.1~15.5GHz, 15.9~18GHz)	5	[81]
	Ti_3C_2 nano-sheets	-40@7.8GHz@2mm	6.8GHz(11.2~18GHz)	2	[120]
	C/TiO_2	-36@15.5GHz@1.6mm	5.6GHz(12.4~18GHz)	1.7	[82]
MXene/dielectric loss materials	$Ti_3C_2T_x$@RGO	-31.2@8.2GHz@2.05mm	5.4GHz (11.4~16.8 GHz)	2.05	[121]
	CNTs/Ti_3C_2-SA foam	-40	4.2GHz(8.2~12.4GHz)	3.95	[122]
	$Ti_3C_2T_x$/CNT hybrids	-52.9@7.15GHz@2.65mm	4.46GHz	1.55	[123]
	MXene/PANI	-56.3@13.8GHz@1.8mm	5.95 GHz	2.4	[124]
	$Ti_3C_2T_X$/SiCnws	-55.7@9 GHz@3.7mm	4.2 GHz	3.5~3.8	[125]
MXene/magnetic loss materials	Ti_3C_2/Ni	-24.3@9.8 GHz@2.2mm	2.6 GHz (8.66~11.26GHz)	2.2	[102]
	Ni@MXene	-52.6@8.4GHz@3mm	6.1GHz	3	[4]
	MXene/Ni	-50.5@5.5GHz@3.5mm	5.28GHz	3.5	[104]
	$Ti_3C_2T_x$ MXene/Ni Chain	-49.9@11.9GHz@1.75mm	2.1GHz	1.75	[103]

	$CoFe@Ti_3C_2T_x$ composites	-36.29@8.56GHz@2.2mm	2.64GHz(10.32~12.96GHz)	1.7	[22]
	$Ti_3C_2T_X$/Ni-spheres	-47.06@12.4GHz@1.5mm	3.6GHz(10.8~14.4GHz)	1.5	[23]
	FeCo-Ti_3C_2 MXene	-17.86@1.6mm	8.8GHz(9.2~18GHz)	1.6	[105]
	Ni-modified Ti_3C_2 MXene	-22.5@11.2GHz@2mm	6.3GHz	1.5	[126]
	MXene/Fe_3O_4	-50.6@13.8 GHz@2mm	4.67 GHz	2	[127]
	$Fe_3O_4@Ti_3C_2T_x$	-57.2@15.7GHz@4.2mm	1.4GHz	4.2	[128]
	MXene/Co_3O_4 composite	−55.4@5.47 GHz@5.5 mm	6.2 GHz (10.8–17 GHz)	2	[3]
	$Ti_3C_2T_x$/CNZF	-58.4@6.2GHz@3.6mm	2.2GHz(3.8~6GHz)	4.2	[129]
	$NiFe_2O_4$-$Ti_3C_2T_x$	-34@13.92GHz@1.7mm	7.68GHz (10.32-18GHz)	1.5	[130]
	$Ti_3C_2T_x@NiCo_2O_4$	-50.96@12.24GHz@2.18 mm	-	-	[131]
	$CoFe_2O_4$-Ti_3C_2	-30.9@11.9GHz@1.5mm	8.5GHz(8.3~16.8GHz)	1.5	[132]
	Ti_3C_2 MXene/FCI composites	-15.52 @12.8 GHz @1mm	8.16 GHz (9.84-18GHz)	1	[21]
MXene/multiple loss materials	$Ti_3C_2T_X$/CNZFO/PANI	-37.1@10.2GHz@2.2mm	4.1GHz(8.2~12.3GHz)	2.2	[136]
	Ti_3C_2/Fe_3O_4/PANI	-40.3@15.3GHz@1.9mm	5.2GHz(12.8~18GHz)	1.9	[137]
	PVB/$Ba_3Co_2Fe_{24}O_{41}$/Ti_3C_2	-46.3@5.8GHz@2.8mm	1.6GHz	2.8	[138]
	Ni/TiO_2/C	-31.91@16.93GHz@1.4mm	3.04GHz(14.24~17.28GHz)	1.5	[139]
	Fe&TiO_2@C	-51.8@6.6GHz@3mm	6.5GHz(11.5~18GHz)	1.6	[140]

During the last ten years, the MXene-based MAMs have made significant progress in design, fabrication and application. The fabrication method includes HF acid etching, fluorine salt etching and molten salt etching. Among these methods, fluorine salt etching is the most widely used way. More safe and high yield fabrication methods are urgent need for the application in the field of MA.

The comparison of different kinds of MXene-based MAMs are shown in Table 2. For pure MXene, the MA performance is determined by ratio of matrix, the interlayer space and morphology. All these can be tuned by the condition of exfoliating, such as reactant concentration, reaction time, and reaction temperature. Though the conductivity of MXene is much higher than other 2D materials, they usually result in poor impedance matching. So the shortcomings can be compensated by introducing other lossy materials. The synergistic effect between MXene and dielectric loss material/magnetic loss material will improve the MA performance. There are several ways to improve the MA performance of MXene-based material: 1) By optimizing the synthesis conditions, the specific surface area of MXene and MXene-based materials can be increased, so the interface polarization was induced. 2) As is mentioned above, the electromagnetic matching ability can be optimized by introducing materials with different loss mechanisms to improve the attenuation of EMWs. 3) It is very important to improve both RL and EAB, not just one of them. So strong loss ability and good impedance matching is the key to achieving the goal of “thin, lightweight, wide and strong”.

6、Summary

In this paper, the recent progress of MXene and MXene-based MAMs has been reviewed. MXene, as a new kind of 2D material, has exhibited many advantages as MAMs such as special layered structure, high electrical conductivity and high specific surface area. So MXene-based composite as MAMs also have the characteristics of tunable structure, simple preparation and good stability. In general, MXene usually coupled with other dielectric loss materials or magnetic loss materials to reduce the permittivity or increase the permeability, and then improve the impedance matching, in order to achieve the purpose of MA attenuation. The synergetic effects between MXene and the other loss material will create more loss mechanisms, which benefit to the MA performance. The method of MXene coupled with multiple loss material is also a popular trend for developing high-performance MAMs.

MXene and MXene-based MAMs have achieved great progress in recent years. However, MXene-based composite MAMs are still in the research stage and will show different advantages when combined with various composite materials. In the future, the absorbing mechanism of various MXene-based composite MAMs should be systematically studied. Firstly, more efforts should be made on the research of preparation, structure optimization in order to improve MA performance. Secondly, MXene-based multiple loss materials as MAMs should be further studied to achieve multiple mechanisms of loss of MA. Thirdly, “thin, wide, light, strong” is the developing direction of MXene and MXene-based MAMs, especially in military field. Finally, MXene-based materials have already shown the potential as advanced MAMs.

We firmly believe that with our efforts, MXene-based MAMs will make greater progress in the future.

Acknowledgements

The authors gratefully acknowledge the financial support from MOST (2016YFA0200200), NSFC (21374050, 51373078, and 51422304), and NSF of Tianjin City (15JCYBJC17700).

Conflict of Interest

The authors declare no conflict of interest.

Reference

[1] Z. Wang, Z. Cheng, C. Fang, X. Hou, L. Xie, Recent advances in MXenes composites for electromagnetic interference shielding and microwave absorption. Composites Part A: Applied Science and Manufacturing 136 (2020) 105956.

[2] W. Gu, J. Lv, B. Quan, X. Liang, B. Zhang, G. Ji, Achieving MOF-derived one-dimensional porous ZnO/C nanofiber with lightweight and enhanced microwave response by an electrospinning method. Journal of Alloys and Compounds 806 (2019) 983-991.

[3] R. Deng, B. Chen, H. Li, K. Zhang, T. Zhang, Y. Yu, et al., MXene/Co3O4 composite material: Stable synthesis and its enhanced broadband microwave absorption. Applied Surface Science 488 (2019) 921-930.

[4] L. Liang, R. Yang, G. Han, Y. Feng, B. Zhao, R. Zhang, et al., Enhanced Electromagnetic Wave-Absorbing Performance of Magnetic Nanoparticles-Anchored 2D Ti3C2Tx MXene. Acs Applied Materials & Interfaces 12 (2) (2020) 2644-2654.

[5] L. Wang, X. Yu, X. Li, J. Zhang, M. Wang, R. Che, MOF-derived yolk-shell Ni@C@ZnO Schottky contact structure for enhanced microwave absorption. Chemical Engineering Journal 383 (2020).

[6] X. Zhang, J. Qao, J. Zhao, D. Xu, F. Wang, C. Liu, et al., High-Efficiency Electromagnetic Wave Absorption of Cobalt Decorated NH2-UIO-66-Derived Porous ZrO2/C. Acs Applied Materials & Interfaces 11 (39) (2019) 35959-35968.

[7] X. Xiao, W. Zhu, Z. Tan, W. Tian, Y. Guo, H. Wang, et al., Ultra-small Co/CNTs nanohybrid from metal organic framework with highly efficient microwave absorption. Composites Part B-Engineering 152 (2018) 316-323.

[8] R. Yang, J. Yuan, C. Yu, K. Yan, Y. Fu, H. Xie, et al., Efficient electromagnetic wave absorption by SiC/Ni/NiO/C nanocomposites. Journal of Alloys and Compounds 816 (2020).

[9] X. Sun, X. Lv, M. Sui, X. Weng, X. Li, J. Wang, Decorating MOF-Derived Nanoporous Co/C in Chain-Like Polypyrrole (PPy) Aerogel: A Lightweight Material with Excellent Electromagnetic Absorption. Materials 11 (5) (2018).

[10] Y. Qi, P. Yin, L. Zhang, J. Wang, X. Feng, K. Wang, et al., Novel Microwave Absorber of NixMn1-xFe2O4/Carbonized Chaff (x=0.3, 0.5, and 0.7) Based on Biomass. Acs Omega 4 (7) (2019) 12376-12384.

[11] T. Bai, Y. Guo, H. Liu, G. Song, D. Zhang, Y. Wang, et al., Achieving enhanced electromagnetic shielding and absorption capacity of cellulose-derived carbon aerogels via tuning the carbonization temperature. Journal Of Materials Chemistry C 8 (15) (2020) 5191-5201.

[12] Y. Fang, W. Xue, R. Zhao, S. Bao, W. Wang, L. Sun, et al., Effect of nanoporosity on the electromagnetic wave absorption performance in a biomass-templated Fe3O4/C composite: a small-angle neutron scattering study. Journal Of Materials Chemistry C 8 (1) (2020) 319-327.

[13] P. Hu, S. Dong, X. Li, J. Chen, X. Zhang, P. Hu, et al., A low-cost strategy to synthesize MnO nanorods anchored on 3D biomass-derived carbon with superior microwave absorption properties. Journal Of Materials Chemistry C 7 (30) (2019) 9219-9228.

[14] H. Zhao, Y. Cheng, W. Liu, L. Yang, B. Zhang, L. P. Wang, et al., Biomass-Derived Porous Carbon-Based Nanostructures for Microwave Absorption. Nano-Micro Letters 11 (1) (2019).

[15] L. Liu, S. Yang, H. Hu, T. Zhang, Y. Yuan, Y. Li, et al., Lightweight and Efficient Microwave-Absorbing Materials Based on Loofah-Sponge-Derived Hierarchically Porous Carbons. Acs Sustainable Chemistry & Engineering 7 (1) (2019) 1228-1238.

[16] K. Zhang, F. Wu, A. Xie, M. Sun, W. Dong, In Situ Stringing of Metal Organic Frameworks by SiC Nanowires for High-Performance Electromagnetic Radiation Elimination. Acs Applied Materials & Interfaces 9 (38) (2017) 33041-33048.

[17] G. Shao, J. Liang, W. Zhao, B. Zhao, W. Liu, H. Wang, et al., Co decorated polymer-derived SiCN ceramic aerogel composites with ultrabroad microwave absorption performance. Journal of Alloys and Compounds 813 (2020).

[18] Y. Jiao, J. Li, A. Xie, F. Wu, K. Zhang, W. Dong, et al., Confined polymerization strategy to construct polypyrrole/zeolitic imidazolate frameworks (PPy/ZIFs)

nanocomposites for tunable electrical conductivity and excellent electromagnetic absorption. Composites Science and Technology 174 (2019) 232-240.

[19] H. Xu, X. Yin, X. Li, M. Li, S. Liang, L. Zhang, et al., Lightweight Ti2CTx MXene/Poly(vinyl alcohol) Composite Foams for Electromagnetic Wave Shielding with Absorption-Dominated Feature. Acs Applied Materials & Interfaces 11 (10) (2019) 10198-10207.

[20] Y. Qing, D. Min, Y. Zhou, F. Luo, W. Zhou, Graphene nanosheet- and flake carbonyl iron particle-filled epoxy-silicone composites as thin-thickness and wide-bandwidth microwave absorber. Carbon 86 (2015) 98-107.

[21] S. Yan, C. Cao, J. He, L. He, Z. Qu, Investigation on the electromagnetic and broadband microwave absorption properties of Ti3C2 Mxene/flaky carbonyl iron composites. Journal Of Materials Science-Materials In Electronics 30 (7) (2019) 6537-6543.

[22] C. Zhou, X. Wang, H. Luo, L. Deng, S. Wang, S. Wei, et al., Interfacial design of sandwich-like CoFe@Ti3C2Tx composites as high efficient microwave absorption materials. Applied Surface Science 494 (2019) 540-550.

[23] N. Li, X. Xie, H. Lu, B. Fan, X. Wang, B. Zhao, et al., Novel two-dimensional Ti3C2Tx/Ni-spheres hybrids with enhanced microwave absorption properties. Ceramics International 45 (17) (2019) 22880-22888.

[24] O. Balci, E. O. Polat, N. Kakenov, C. Kocabas, Graphene-enabled electrically switchable radar-absorbing surfaces. Nature Communications 6 (2015).

[25] F. Meng, H. Wang, F. Huang, Y. Guo, Z. Wang, D. Hui, et al., Graphene-based microwave absorbing composites: A review and prospective. Composites Part B-Engineering 137 (2018) 260-277.

[26] Y. Wang, D. Chen, X. Yin, P. Xu, F. Wu, M. He, Hybrid of MoS2 and Reduced Graphene Oxide: A Lightweight and Broadband Electromagnetic Wave Absorber. Acs Applied Materials & Interfaces 7 (47) (2015) 26226-26234.

[27] J. Y. Yu, F. L. Chi, Y. P. Sun, J. J. Guo, X. G. Liu, Assembled porous Fe3O4@g-C3N4 hybrid nanocomposites with multiple interface polarization for

stable microwave absorption. Ceramics International 44 (16) (2018) 19207-19216.

[28] Y. Qing, W. Zhou, F. Luo, D. Zhu, Titanium carbide (MXene) nanosheets as promising microwave absorbers. Ceramics International 42 (14) (2016) 16412-16416.

[29] P. Liu, Z. Yao, V. M. H. Ng, J. Zhou, L. B. Kong, Novel multilayer-like structure of Ti3C2Tx/CNZF composites for low-frequency electromagnetic absorption. Materials Letters 248 (2019) 214-217.

[30] K. Li, H. Sun, X. Zhang, S. Zhang, H. Dong, C. Zhu, et al., Micro-nanospheres assembled with helically coiled nitrogen-doped carbon nanotubes: Fabrication and microwave absorption properties. Materials & Design 186 (2020).

[31] C. Li, H. Song, X. Jiang, Z. Zhang, L. Yu, An efficient high-frequency electromagnetic wave absorber: Nickel-N@Carbon composite. Journal of Alloys and Compounds 814 (2020).

[32] G. Cui, X. Zheng, X. Lv, Q. Jia, W. Xie, G. Gu, Synthesis and microwave absorption of Ti3C2Tx MXene with diverse reactant concentration, reaction time, and reaction temperature. Ceramics International 45 (17) (2019) 23600-23610.

[33] K.-L. Zhang, J.-Y. Zhang, Z.-L. Hou, S. Bi, Q.-L. Zhao, Multifunctional broadband microwave absorption of flexible graphene composites. Carbon 141 (2019) 608-617.

[34] M. Naguib, M. Kurtoglu, V. Presser, J. Lu, J. Niu, M. Heon, et al., Two□Dimensional Nanocrystals: Two□Dimensional Nanocrystals Produced by Exfoliation of Ti3AlC2 (Adv. Mater. 37/2011). Advanced Materials 23 (37) (2011) 4207-4207.

[35] M. Naguib, O. Mashtalir, J. Carle, V. Presser, J. Lu, L. Hultman, et al., Two-Dimensional Transition Metal Carbides. Acs Nano 6 (2) (2012) 1322-1331.

[36] H. Kumar, N. C. Frey, L. Dong, B. Anasori, Y. Gogotsi, V. B. Shenoy, Tunable Magnetism and Transport Properties in Nitride MXenes. Acs Nano 11 (8) (2017) 7648-7655.

[37] O. Mashtalir, M. Naguib, V. N. Mochalin, Y. Dall'Agnese, M. Heon, M. W. Barsoum, et al., Intercalation and delamination of layered carbides and carbonitrides. Nature Communications 4 (1) (2013) 1716.

[38]M. Ghidiu, M. R. Lukatskaya, M.-Q. Zhao, Y. Gogotsi, M. W. Barsoum, Conductive two-dimensional titanium carbide 'clay' with high volumetric capacitance. Nature 516 (7529) (2014) 78-81.

[39]B. Anasori, Y. Xie, M. Beidaghi, J. Lu, B. C. Hosler, L. Hultman, et al., Two-Dimensional, Ordered, Double Transition Metals Carbides (MXenes). Acs Nano 9 (10) (2015) 9507-9516.

[40]G. Zou, Z. Zhang, J. Guo, B. Liu, Q. Zhang, C. Fernandez, et al., Synthesis of MXene/Ag Composites for Extraordinary Long Cycle Lifetime Lithium Storage at High Rates. Acs Applied Materials & Interfaces 8 (34) (2016) 22280-22286.

[41]M. Alhabeb, K. Maleski, B. Anasori, P. Lelyukh, L. Clark, S. Sin, et al., Guidelines for Synthesis and Processing of Two-Dimensional Titanium Carbide (Ti3C2Tx MXene). Chemistry of Materials 29 (18) (2017) 7633-7644.

[42]Y. Li, H. Shao, Z. Lin, J. Lu, L. Liu, B. Duployer, et al., A general Lewis acidic etching route for preparing MXenes with enhanced electrochemical performance in non-aqueous electrolyte. Nature Materials (2020).

[43]M. Khazaei, A. Mishra, N. S. Venkataramanan, A. K. Singh, S. Yunoki, Recent advances in MXenes: From fundamentals to applications. Current Opinion in Solid State & Materials Science 23 (3) (2019) 164-178.

[44]J. Pang, R. G. Mendes, A. Bachmatiuk, L. Zhao, H. Q. Ta, T. Gemming, et al., Applications of 2D MXenes in energy conversion and storage systems. Chemical Society Reviews 48 (1) (2019) 72-133.

[45]Y.-T. Liu, P. Zhang, N. Sun, B. Anasori, Q.-Z. Zhu, H. Liu, et al., Self-Assembly of Transition Metal Oxide Nanostructures on MXene Nanosheets for Fast and Stable Lithium Storage. Advanced Materials 30 (23) (2018).

[46]J. P. Fei, S. W. Koh, W. G. Tu, J. Y. Ge, H. Rezaeyan, S. Hou, et al., Functionalized MXene Enabled Sustainable Water Harvesting and Desalination. Advanced Sustainable Systems.

[47]X. Y. Wang, Q. Q. Li, J. F. Zhang, H. M. Huang, S. Y. Wu, Y. Yang, Novel thin-film reverse osmosis membrane with MXene Ti3C2Tx embedded in polyamide

to enhance the water flux, anti-fouling and chlorine resistance for water desalination. Journal Of Membrane Science 603 (2020) 12.

[48] Y. N. Yang, Z. R. Cao, P. He, L. J. Shi, G. Q. Ding, R. R. Wang, et al., Ti3C2Tx MXene-graphene composite films for wearable strain sensors featured with high sensitivity and large range of linear response. Nano Energy 66 (2019).

[49] R. Kumar, S. Pal, Y. K. Prajapati, J. P. Saini, Sensitivity Enhancement of MXene Based SPR Sensor Using Silicon: Theoretical Analysis. Silicon.

[50] T. Y. Ma, J. L. Cao, M. Jaroniec, S. Z. Qiao, Interacting Carbon Nitride and Titanium Carbide Nanosheets for High-Performance Oxygen Evolution. Angewandte Chemie-International Edition 55 (3) (2016) 1138-1142.

[51] A. D. Handoko, S. N. Steinmann, Z. W. Seh, Theory-guided materials design: two-dimensional MXenes in electro- and photocatalysis. Nanoscale Horizons 4 (4) (2019) 809-827.

[52] P. Collini, S. Kota, A. D. Dillon, M. W. Barsoum, A. T. Fafarman, Electrophoretic Deposition of Two-Dimensional Titanium Carbide (MXene) Thick Films. Journal of the Electrochemical Society 164 (9) (2017) D573-D580.

[53] P. He, M.-S. Cao, Y.-Z. Cai, J.-C. Shu, W.-Q. Cao, J. Yuan, Self-assembling flexible 2D carbide MXene film with tunable integrated electron migration and group relaxation toward energy storage and green EMI shielding. Carbon 157 (2020) 80-89.

[54] F. Shahzad, M. Alhabeb, C. B. Hatter, B. Anasori, S. M. Hong, C. M. Koo, et al., Electromagnetic interference shielding with 2D transition metal carbides (MXenes). Science 353 (6304) (2016) 1137-1140.

[55] A. Iqbal, F. Shahzad, K. Hantanasirisakul, M.-K. Kim, J. Kwon, J. Hong, et al., Anomalous absorption of electromagnetic waves by 2D transition metal carbonitride Ti₃CNT_x (MXene). Science 369 (6502) (2020) 446.

[56] Y. Qian, H. Wei, J. Dong, Y. Du, X. Fang, W. Zheng, et al., Fabrication of urchin-like ZnO-MXene nanocomposites for high-performance electromagnetic absorption. Ceramics International 43 (14) (2017) 10757-10762.

[57]G. Zhao, H. Lv, Y. Zhou, X. Zheng, C. Wu, C. Xu, Self-Assembled Sandwich-like MXene-Derived Nanocomposites for Enhanced Electromagnetic Wave Absorption. Acs Applied Materials & Interfaces 10 (49) (2018) 42925-42932.

[58]Q. Tang, Z. Zhou, P. Shen, Are MXenes Promising Anode Materials for Li Ion Batteries? Computational Studies on Electronic Properties and Li Storage Capability of Ti3C2 and Ti3C2X2 (X = F, OH) Monolayer. Journal of the American Chemical Society 134 (40) (2012) 16909-16916.

[59]P. Srivastava, A. Mishra, H. Mizuseki, K.-R. Lee, A. K. Singh, Mechanistic Insight into the Chemical Exfoliation and Functionalization of Ti3C2 MXene. Acs Applied Materials & Interfaces 8 (36) (2016) 24256-24264.

[60]M. Naguib, M. Kurtoglu, V. Presser, J. Lu, J. Niu, M. Heon, et al., Two-Dimensional Nanocrystals: Two-Dimensional Nanocrystals Produced by Exfoliation of Ti3AlC2 (Adv. Mater. 37/2011). Advanced Materials 23 (37) (2011) 4207-4207.

[61]W. Xin, G.-Q. Xi, W.-T. Cao, C. Ma, T. Liu, M.-G. Ma, et al., Lightweight and flexible MXene/CNF/silver composite membranes with a brick-like structure and high-performance electromagnetic-interference shielding. Rsc Advances 9 (51) (2019) 29636-29644.

[62]F. Xie, F. Jia, L. Zhuo, Z. Lu, L. Si, J. Huang, et al., Ultrathin MXene/aramid nanofiber composite paper with excellent mechanical properties for efficient electromagnetic interference shielding. Nanoscale 11 (48) (2019) 23382-23391.

[63]P. Sambyal, A. Iqbal, J. Hong, H. Kim, M.-K. Kim, S. M. Hong, et al., Ultralight and Mechanically Robust Ti3C2Tx Hybrid Aerogel Reinforced by Carbon Nanotubes for Electromagnetic Interference Shielding. Acs Applied Materials & Interfaces 11 (41) (2019) 38046-38054.

[64]K. Maleski, V. N. Mochalin, Y. Gogotsi, Dispersions of Two-Dimensional Titanium Carbide MXene in Organic Solvents. Chemistry of Materials 29 (4) (2017) 1632-1640.

[65]G. Sharma, E. Muthuswamy, M. Naguib, Y. Gogotsi, A. Navrotsky, D. Wu,

Calorimetric Study of Alkali Metal Ion (K+, Na+, Li+) Exchange in a Clay-Like MXene. The Journal of Physical Chemistry C 121 (28) (2017) 15145-15153.

[66] H. Wang, J. Zhang, Y. Wu, H. Huang, G. Li, X. Zhang, et al., Surface modified MXene Ti3C2 multilayers by aryl diazonium salts leading to large-scale delamination. Applied Surface Science 384 (2016) 287-293.

[67] T. Zhang, L. Pan, H. Tang, F. Du, Y. Guo, T. Qiu, et al., Synthesis of two-dimensional Ti3C2Tx MXene using HCl+LiF etchant: Enhanced exfoliation and delamination. Journal of Alloys and Compounds 695 (2017) 818-826.

[68] J. Peng, X. Chen, W.-J. Ong, X. Zhao, N. Li, Surface and Heterointerface Engineering of 2D MXenes and Their Nanocomposites: Insights into Electro- and Photocatalysis. Chem 5 (1) (2019) 18-50.

[69] P. Urbankowski, B. Anasori, T. Makaryan, D. Er, S. Kota, P. L. Walsh, et al., Synthesis of two-dimensional titanium nitride Ti4N3 (MXene). Nanoscale 8 (22) (2016) 11385-11391.

[70] Y. Li, H. Shao, Z. Lin, J. Lu, L. Liu, B. Duployer, et al., A general Lewis acidic etching route for preparing MXenes with enhanced electrochemical performance in non-aqueous electrolyte. Nature Materials 19 (8) (2020) 894-899.

[71] A. Lipatov, M. Alhabeb, M. R. Lukatskaya, A. Boson, Y. Gogotsi, A. Sinitskii, Effect of Synthesis on Quality, Electronic Properties and Environmental Stability of Individual Monolayer Ti3C2 MXene Flakes. Advanced Electronic Materials 2 (12) (2016) 1600255.

[72] C. J. Zhang, B. Anasori, A. Seral-Ascaso, S.-H. Park, N. McEvoy, A. Shmeliov, et al., Transparent, Flexible, and Conductive 2D Titanium Carbide (MXene) Films with High Volumetric Capacitance. Advanced materials (Deerfield Beach, Fla.) 29 (36) (2017).

[73] Z. Ling, C. E. Ren, M. Q. Zhao, J. Yang, J. M. Giammarco, J. S. Qiu, et al., Flexible and conductive MXene films and nanocomposites with high capacitance. Proceedings of the National Academy of Sciences of the United States of America 111 (47) (2014) 16676-16681.

[74] H. B. Wang, Y. P. Wu, J. F. Zhang, G. Y. Li, H. J. Huang, X. Zhang, et al., Enhancement of the electrical properties of MXene Ti3C2 nanosheets by post-treatments of alkalization and calcination. Materials Letters 160 (2015) 537-540.

[75] A. D. Dillon, M. J. Ghidiu, A. L. Krick, J. Griggs, S. J. May, Y. Gogotsi, et al., Highly Conductive Optical Quality Solution-Processed Films of 2D Titanium Carbide. Advanced Functional Materials 26 (23) (2016) 4162-4168.

[76] T. Zhang, L. M. Pan, H. Tang, F. Du, Y. H. Guo, T. Qiu, et al., Synthesis of two-dimensional Ti3C2Tx MXene using HCl plus LiF etchant: Enhanced exfoliation and delamination. Journal of Alloys and Compounds 695 (2017) 818-826.

[77] B. Fan, N. Li, B. Dai, S. Shang, L. Guan, B. Zhao, et al., Investigation of adjacent spacing dependent microwave absorption properties of lamellar structural Ti3C2Tx MXenes. Advanced Powder Technology 31 (2) (2020) 808-815.

[78] G. Cui, X. Sun, G. Zhang, Z. Zhang, H. Liu, J. Gu, et al., Electromagnetic absorption performance of two-dimensional MXene Ti3C2Tx exfoliated by HCl plus LiF etchant with diverse etching times. Materials Letters 252 (2019) 8-10.

[79] Z. Zhang, Y. He, Y. Lv, L. Zhang, X. Chen, Z. Wu, et al., Effect of Surface Structure and Composition on the Electromagnetic Properties of Ti3C2Tx MXenes for Highly Efficient Electromagnetic Wave Absorption. Journal Of Physical Chemistry C 124 (36) (2020) 19666-19674.

[80] G. Xu, X. Wang, S. Gong, S. Wei, J. Liu, Y. Xu, Solvent-regulated preparation of well-intercalated Ti3C2Tx MXene nanosheets and application for highly effective electromagnetic wave absorption. Nanotechnology 29 (35) (2018).

[81] X. Li, X. Yin, M. Han, C. Song, X. Sun, H. Xu, et al., A controllable heterogeneous structure and electromagnetic wave absorption properties of Ti2CTx MXene. Journal Of Materials Chemistry C 5 (30) (2017) 7621-7628.

[82] M. Han, X. Yin, X. Li, B. Anasori, L. Zhang, L. Cheng, et al., Laminated and Two-Dimensional Carbon-Supported Microwave Absorbers Derived from MXenes. Acs Applied Materials & Interfaces 9 (23) (2017) 20038-20045.

[83] N. Wu, D. Xu, Z. Wang, F. Wang, J. Liu, W. Liu, et al., Achieving superior

electromagnetic wave absorbers through the novel metal-organic frameworks derived magnetic porous carbon nanorods. Carbon 145 (2019) 433-444.

[84] P. Liu, Y. Zhang, J. Yan, Y. Huang, L. Xia, Z. Guang, Synthesis of lightweight N-doped graphene foams with open reticular structure for high-efficiency electromagnetic wave absorption. Chemical Engineering Journal 368 (2019) 285-298.

[85] Y. Qiu, Y. Lin, H. Yang, L. Wang, M. Wang, B. Wen, Hollow Ni/C microspheres derived from Ni-metal organic framework for electromagnetic wave absorption. Chemical Engineering Journal 383 (2020).

[86] X. F. Zhou, Z. R. Jia, A. L. Feng, X. X. Wang, J. J. Liu, M. Zhang, et al., Synthesis of fish skin-derived 3D carbon foams with broadened bandwidth and excellent electromagnetic wave absorption performance. Carbon 152 (2019) 827-836.

[87] M. Zeng, Q. Cao, J. Liu, B. Guo, X. Hao, Q. Liu, et al., Hierarchical Cobalt Selenides as Highly Efficient Microwave Absorbers with Tunable Frequency Response. Acs Applied Materials & Interfaces 12 (1) (2020) 1222-1231.

[88] M.-S. Cao, J. Yang, W.-L. Song, D.-Q. Zhang, B. Wen, H.-B. Jin, et al., Ferroferric Oxide/Multiwalled Carbon Nanotube vs Polyaniline/Ferroferric Oxide/Multiwalled Carbon Nanotube Multiheterostructures for Highly Effective Microwave Absorption. Acs Applied Materials & Interfaces 4 (12) (2012) 6949-6956.

[89] C. Wang, X. Han, P. Xu, X. Zhang, Y. Du, S. Hu, et al., The electromagnetic property of chemically reduced graphene oxide and its application as microwave absorbing material. Applied Physics Letters 98 (7) (2011).

[90] R. Shu, W. Li, Y. Wu, J. Zhang, G. Zhang, Nitrogen-doped Co-C/MWCNTs nanocomposites derived from bimetallic metal-organic frameworks for electromagnetic wave absorption in the X-band. Chemical Engineering Journal 362 (2019) 513-524.

[91] Z. Yang, Y. Zhang, M. Li, L. Yang, J. Liu, Y. Hou, et al., Surface Architecture of Ni-Based Metal Organic Framework Hollow Spheres for Adjustable Microwave Absorption. Acs Applied Nano Materials 2 (12) (2019) 7888-7897.

[92] X. Liang, Z. Man, B. Quan, J. Zheng, W. Gu, Z. Zhang, et al.,

Environment-Stable CoxNiy Encapsulation in Stacked Porous Carbon Nanosheets for Enhanced Microwave Absorption. Nano-Micro Letters 12 (1) (2020) 102.

[93] H. Wang, F. Meng, F. Huang, C. Jing, Y. Li, W. Wei, et al., Interface Modulating CNTs@PANi Hybrids by Controlled Unzipping of the Walls of CNTs To Achieve Tunable High-Performance Microwave Absorption. Acs Applied Materials & Interfaces 11 (12) (2019) 12142-12153.

[94] Z. Zhang, Q. Zhu, X. Chen, Z. Wu, Y. He, Y. Lv, et al., Ni@C composites derived from Ni-based metal organic frameworks with a lightweight, ultrathin, broadband and highly efficient microwave absorbing properties. Applied Physics Express 12 (1) (2019).

[95] J. Yu, R. Su, J. Yu, X. Liu, X. Zhang, X. Dong, Regulation of dielectric loss by different exposed crystal facets in graphite-coated titanium carbide nanocomposites. Ceramics International 46 (11) (2020) 18339-18346.

[96] L. J. Yang, H. L. Lv, M. Li, Y. Zhang, J. C. Liu, Z. H. Yang, Multiple polarization effect of shell evolution on hierarchical hollow C@MnO2 composites and their wideband electromagnetic wave absorption properties. Chemical Engineering Journal 392 (2020) 10.

[97] Q. Liu, X. Liu, H. Feng, H. Shui, R. Yu, Metal organic framework-derived Fe/carbon porous composite with low Fe content for lightweight and highly efficient electromagnetic wave absorber. Chemical Engineering Journal 314 (2017) 320-327.

[98] N. Li, G.-W. Huang, Y.-Q. Li, H.-M. Xiao, Q.-P. Feng, N. Hu, et al., Enhanced Microwave Absorption Performance of Coated Carbon Nanotubes by Optimizing the Fe3O4 Nanocoating Structure. Acs Applied Materials & Interfaces 9 (3) (2017) 2973-2983.

[99] Y. Cheng, J. Z. Y. Seow, H. Zhao, Z. J. Xu, G. Ji, A Flexible and Lightweight Biomass-Reinforced Microwave Absorber. Nano-Micro Letters 12 (1) (2020) 125.

[100] Y. Zhang, X. Wang, M. Cao, Confinedly implanted NiFe2O4-rGO: Cluster tailoring and highly tunable electromagnetic properties for selective-frequency microwave absorption. Nano Research 11 (3) (2018) 1426-1436.

[101] Q. Song, F. Ye, L. Kong, Q. Shen, L. Han, L. Feng, et al., Graphene and MXene Nanomaterials: Toward High-Performance Electromagnetic Wave Absorption in Gigahertz Band Range. Advanced Functional Materials 30 (31) (2020).

[102] Y. Liu, S. Zhang, X. Su, J. Xu, Y. Li, Enhanced microwave absorption properties of Ti3C2 MXene powders decorated with Ni particles. Journal Of Materials Science (2020).

[103] L. Liang, G. Han, Y. Li, B. Zhao, B. Zhou, Y. Feng, et al., Promising Ti3C2Tx MXene/Ni Chain Hybrid with Excellent Electromagnetic Wave Absorption and Shielding Capacity. Acs Applied Materials & Interfaces 11 (28) (2019) 25399-25409.

[104] X. Li, W. You, L. Wang, J. Liu, Z. Wu, K. Pei, et al., Self-Assembly-Magnetized MXene Avoid Dual-Agglomeration with Enhanced Interfaces for Strong Microwave Absorption through a Tunable Electromagnetic Property. Acs Applied Materials & Interfaces 11 (47) (2019) 44536-44544.

[105] J. He, D. Shan, S. Yan, H. Luo, C. Cao, Y. Peng, Magnetic FeCo nanoparticles-decorated Ti3C2 MXene with enhanced microwave absorption performance. Journal of Magnetism and Magnetic Materials 492 (2019).

[106] W. Feng, H. Luo, Y. Wang, S. Zeng, Y. Tan, L. Deng, et al., Mxenes Derived Laminated and Magnetic Composites with Excellent Microwave Absorbing Performance. Scientific Reports 9 (2019).

[107] P. Liu, Z. Yao, V. M. H. Ng, J. Zhou, L. B. Kong, K. Yue, Facile synthesis of ultrasmall Fe3O4 nanoparticles on MXenes for high microwave absorption performance. Composites Part a-Applied Science And Manufacturing 115 (2018) 371-382.

[108] H. Wang, L. Xiang, W. Wei, J. An, J. He, C. Gong, et al., Efficient and Lightweight Electromagnetic Wave Absorber Derived from Metal Organic Framework-Encapsulated Cobalt Nanoparticles. Acs Applied Materials & Interfaces 9 (48) (2017) 42102-42110.

[109] C.-L. Zhu, M.-L. Zhang, Y.-J. Qiao, G. Xiao, F. Zhang, Y.-J. Chen,

Fe3O4/TiO2 Core/Shell Nanotubes: Synthesis and Magnetic and Electromagnetic Wave Absorption Characteristics. Journal Of Physical Chemistry C 114 (39) (2010) 16229-16235.

[110] D. Xu, X. Xiong, P. Chen, Q. Yu, H. Chu, S. Yang, et al., Superior corrosion-resistant 3D porous magnetic graphene foam-ferrite nanocomposite with tunable electromagnetic wave absorption properties. Journal of Magnetism and Magnetic Materials 469 (2019) 428-436.

[111] W. Liu, S. Tan, Z. Yang, G. Ji, Enhanced Low-Frequency Electromagnetic Properties of MOF-Derived Cobalt through Interface Design. Acs Applied Materials & Interfaces 10 (37) (2018) 31610-31622.

[112] J. Yan, Y. Huang, Y. Yan, L. Ding, P. Liu, High-Performance Electromagnetic Wave Absorbers Based on Two Kinds of Nickel-Based MOF-Derived Ni@C Microspheres. Acs Applied Materials & Interfaces 11 (43) (2019) 40781-40792.

[113] Z. Li, X. Li, Y. Zong, G. Tan, Y. Sun, Y. Lan, et al., Solvothermal synthesis of nitrogen-doped graphene decorated by superparamagnetic Fe3O4 nanoparticles and their applications as enhanced synergistic microwave absorbers. Carbon 115 (2017) 493-502.

[114] X. Liang, B. Quan, Z. Man, B. Cao, N. Li, C. Wang, et al., Self-Assembly Three-Dimensional Porous Carbon Networks for Efficient Dielectric Attenuation. Acs Applied Materials & Interfaces 11 (33) (2019) 30228-30233.

[115] W. Liu, L. Liu, Z. Yang, J. Xu, Y. Hou, G. Ji, A Versatile Route toward the Electromagnetic Functionalization of Metal–Organic Framework-Derived Three-Dimensional Nanoporous Carbon Composites. Acs Applied Materials & Interfaces 10 (10) (2018) 8965-8975.

[116] R. Wang, M. He, Y. Zhou, S. Nie, Y. Wang, W. Liu, et al., Metal-organic frameworks self-templated cubic hollow Co/N/C@MnO2 composites for electromagnetic wave absorption. Carbon 156 (2020) 378-388.

[117] R. Shu, Z. Wan, J. Zhang, Y. Wu, Y. Liu, J. Shi, et al., Facile Design of Three-Dimensional Nitrogen-Doped Reduced Graphene Oxide/Multi-Walled Carbon

Nanotube Composite Foams as Lightweight and Highly Efficient Microwave Absorbers. Acs Applied Materials & Interfaces 12 (4) (2020) 4689-4698.

[118] J.-P. Chen, H. Jia, Z. Liu, Q.-Q. Kong, Z.-H. Hou, L.-J. Xie, et al., Construction of C-Si heterojunction interface in SiC whisker/reduced graphene oxide aerogels for improving microwave absorption. Carbon 164 (2020) 59-68.

[119] J. Zhang, W. Xue, X.-Y. Chen, Ti3C2Tx MXenes as thin broadband absorbers. Nanotechnology 31 (27) (2020).

[120] W. Feng, H. Luo, Y. Wang, S. Zeng, L. Deng, X. Zhou, et al., Ti3C2 MXene: a promising microwave absorbing material. Rsc Advances 8 (5) (2018) 2398-2403.

[121] L. Wang, H. Liu, X. Lv, G. Cui, G. Gu, Facile synthesis 3D porous MXene Ti3C2Tx@RGO composite aerogel with excellent dielectric loss and electromagnetic wave absorption. Journal of Alloys and Compounds 828 (2020).

[122] X. Liu, N. Chai, Z. Yu, H. Xu, X. Li, J. Liu, et al., Ultra-light, high flexible and efficient CNTs/Ti3C2-sodium alginate foam for electromagnetic absorption application. Journal Of Materials Science & Technology 35 (12) (2019) 2859-2867.

[123] X. Li, X. Yin, M. Han, C. Song, H. Xu, Z. Hou, et al., Ti3C2 MXenes modified with in situ grown carbon nanotubes for enhanced electromagnetic wave absorption properties. Journal Of Materials Chemistry C 5 (16) (2017) 4068-4074.

[124] H. Wei, J. Dong, X. Fang, W. Zheng, Y. Sun, Y. Qian, et al., Ti3C2Tx MXene/polyaniline (PANI) sandwich intercalation structure composites constructed for microwave absorption. Composites Science and Technology 169 (2019) 52-59.

[125] X. Li, X. Yin, H. Xu, M. Han, M. Li, S. Liang, et al., Ultralight MXene-Coated, Interconnected SiCnws Three-Dimensional Lamellar Foams for Efficient Microwave Absorption in the X-Band. Acs Applied Materials & Interfaces 10 (40) (2018) 34524-34533.

[126] W. Feng, H. Luo, S. Zeng, C. Chen, L. Deng, Y. Tan, et al., Ni-modified Ti3C2 MXene with enhanced microwave absorbing ability. Materials Chemistry Frontiers 2 (12) (2018) 2320-2326.

[127] X. Li, M. Zhang, W. You, K. Pei, Q. Zeng, Q. Han, et al., Magnetized MXene

Microspheres with Multiscale Magnetic Coupling and Enhanced Polarized Interfaces for Distinct Microwave Absorption via a Spray-Drying Method. Acs Applied Materials & Interfaces 12 (15) (2020) 18138-18147.

[128] X. Zhang, H. Wang, R. Hu, C. Huang, W. Zhong, L. Pan, et al., Novel solvothermal preparation and enhanced microwave absorption properties of Ti3C2Tx MXene modified by in situ coated Fe3O4 nanoparticles. Applied Surface Science 484 (2019) 383-391.

[129] P. Liu, S. Chen, M. Yao, Z. Yao, V. M. H. Ng, J. Zhou, et al., Delamination strategy to achieve Ti3C2Tx/CNZF composites with tunable electromagnetic absorption. Materials Science in Semiconductor Processing 112 (2020).

[130] D. Shan, J. He, L. Deng, S. Yan, H. Luo, S. Huang, et al., The underlying mechanisms of enhanced microwave absorption performance for the NiFe2O4-decorated Ti3C2Tx MXene. Results In Physics 15 (2019).

[131] T. Hou, B. Wang, M. Ma, A. Feng, Z. Huang, Y. Zhang, et al., Preparation of two-dimensional titanium carbide (Ti3C2Tx) and NiCo2O4 composites to achieve excellent microwave absorption properties. Composites Part B-Engineering 180 (2020).

[132] J. He, S. Liu, L. Deng, D. Shan, C. Cao, H. Luo, et al., Tunable electromagnetic and enhanced microwave absorption properties in CoFe2O4 decorated Ti3C2 MXene composites. Applied Surface Science 504 (2020).

[133] H. Zhuang, X. Wang, J. Wang, M. Guo, D. Tang, B. Zhang, et al., Broadband microwave metamaterial absorber based on magnetic periodic elements. Journal of Physics D: Applied Physics 53 (25) (2020) 255502.

[134] H. Zhao, S. Xu, D. Tang, Y. Yang, B. Zhang, Thin magnetic coating for low-frequency broadband microwave absorption. Journal of Applied Physics 116 (24) (2014) 243911.

[135] O. Khani, M. Z. Shoushtari, K. Ackland, P. Stamenov, The structural, magnetic and microwave properties of spherical and flake shaped carbonyl iron particles as thin multilayer microwave absorbers. Journal of Magnetism and Magnetic

Materials 428 (2017) 28-35.

[136] Y. Lei, Z. Yao, S. Li, J. Zhou, A. A. Haidry, P. Liu, Broadband high-performance electromagnetic wave absorption of Co-doped NiZn ferrite/polyaniline on MXenes. Ceramics International 46 (8) (2020) 10006-10015.

[137] Y. Wang, X. Gao, L. Zhang, X. Wu, Q. Wang, C. Luo, et al., Synthesis of Ti3C2/Fe3O4/PANI hierarchical architecture composite as an efficient wide-band electromagnetic absorber. Applied Surface Science 480 (2019) 830-838.

[138] H. Yang, J. Dai, X. Liu, Y. Lin, J. Wang, L. Wang, et al., Layered PVB/Ba3Co2Fe24O41/Ti3C2 Mxene composite: Enhanced electromagnetic wave absorption properties with high impedance match in a wide frequency range. Materials Chemistry and Physics 200 (2017) 179-186.

[139] C. Zhou, X. Wang, H. Luo, L. Deng, S. Wei, Y. Zheng, et al., Rapid and direct growth of bipyramid TiO2 from Ti3C2Tx MXene to prepare Ni/TiO2/C heterogeneous composites for high-performance microwave absorption. Chemical Engineering Journal 383 (2020).

[140] B. Deng, Z. Xiang, J. Xiong, Z. Liu, L. Yu, W. Lu, Sandwich-Like Fe&TiO2@C Nanocomposites Derived from MXene/Fe-MOFs Hybrids for Electromagnetic Absorption. Nano-Micro Letters 12 (1) (2020).

Declaration of interests

☐ √ The authors declare that they have no known competing financial interests or personal relationships that could have appeared to influence the work reported in this paper.